2009

Forces and Torques on Small Animal Insert Coils

Matthew Aloysius McAlpine

Forces and Torques on Small Animal Insert Coils

(Spine Title: Forces and Torques on Small Animal Insert Coils)

(Thesis Format: Monograph)

by

Matthew Aloysius McAlpine
Graduate Program in Physics

Submitted in partial fulfillment of the requirements for the degree of
Master of Science

School of Graduate and Postdoctoral Studies
The University of Western Ontario
London, Ontario, Canada

THE UNIVERSITY OF WESTERN ONTARIO
SCHOOL OF GRADUATE AND POSTDOCTORAL STUDIES

CERTIFICATE OF EXAMINATION

Supervisor	Examiners
Dr. Blaine Chronik	Dr. Martin Zinke-Allmang
Supervisory Committee	Dr. Giles Santyr
Dr. Martin Zinke-Allmang	Dr. James Wisner
Dr. Eugene Wong	

The thesis by

Matthew Aloysius McAlpine

entitled:

Forces and Torques on Small Animal Insert Coils

is accepted in partial fulfilment of the
requirements for the degree of
Master of Science

Date_____

_____
Chair of the Thesis Examination Board

Abstract:

Magnetic Resonance is a popular imaging modality for research and diagnostic purposes. With the increased usage of smaller localized insert coils needed to provide the resolutions required to image smaller sample sizes, the safety with regards to the Lorentz forces has been investigated. These insert coils are made to be readily interchanged in a MR magnet, and are not often motion stabilized inside the magnet's bore. With the large magnetic fields produced by an MR magnet, the Lorentz forces and torques on an insert coil may become quite large, especially during coil failure. In this study the safety of an insert coil will be investigated under catastrophic electrical failures and coil mis-positions to determine if the Lorentz forces and torques on the insert coil will be large enough to cause coil motion.

Keywords: Magnetic Resonance Imaging, MRI, gradient coils, gradient coil failures, Lorentz force, torque

Acknowledgements

I would like to thank the many people that helped and supported me academically through the course of this Master's thesis.

My sincere gratitude to my supervisor, Dr Blaine Chronik, his understanding of the MR world has been invaluable as I work on increasing my proficiency in the field. His patience as I learned about gradient coils, and the theories involved has helped me a great deal.

I would also like to thank William Handler, without his help in computer programming I might not have completed this project. His insistence that I advance my coding knowledge has helped me grow, and learn to apply new ideas to a project.

Over the past couple years; I have had the chance to work with many bright, young scientists in the Chronik Group. Their help through group meetings and journal clubs, and patience explaining topics to me was a great help as I expanded my knowledge in the field of MRI. I would like to thank Jamu Alford, Parisa Hudson, Kyle Gilbert, Dustin Haw, Chad Harris, Geron Bindseil, Rebecca Feldman, Dr Timothy Scholl as well as a couple outside the group in Dr Martin Houde and Ildiko Beres.

Finally I would like to thank my family and friends as they had to listen to me worry and fret about my project, and offer very kind words of encouragement. Thanks to Mom, Dad, Jenny, Christine, Karen, and Michael and of course you cannot forget the Greens who fed me many a meal that I couldn't afford on my own.

Contents:

List of Figures:

List of Tables

List of Symbols and Abbreviations

a	Radius
A	Cross sectional area
B	Magnetic field
B_o	Main magnetic field
c	Specific heat
E	Electric field
Gx	x-gradient
Gy	y-gradient
Gz	z-gradient
h	Planck's constant
I	Current
J	Current density
k	Boltzmann constant
L	Inductance
l	Length
M	Magnetization
M_{xy}	Transverse Magnetization
M_z	Longitudinal Magnetization
m	Mass
M	Merit
N	Torque
P	Power
q	Charge
Q	Thermal energy
R	Resistance
r_c	Insert coil radius
r_m	Main magnet cold bore radius
r_e	Effective radius of the insert coil
T	Temperature
T_1	Longitudinal recovery time constant
T_2^*	Transverse relaxation time constant
v_d	Drift Velocity
α	Temperature coefficient of resistivity
Υ	Gyromagnetic Ratio
η	Efficiency
ρ	Resistivity
ρ_o	Proton Density
μ	Magnetic Moment
τ	Torque
μ_o	Permeability of Free Space
ω	Frequency of Precession

AR	Aspect Ratio
CCMI	Constrained Current Minimum Inductance
DSV	Diameter Spherical Volume
FOV	Field of View
MR	Magnetic Resonance
MRI	Magnetic Resonance Imaging
ppm	Parts per Million
RF	Radio Frequency

Chapter 1: Introduction

As small animal imaging for research purposes increases in popularity, gradient coils capable of higher switching speeds and greater strength are required to provide the necessary spatial resolution for smaller sample sizes. One method of addressing this need is to develop smaller localized gradient coils and insert them into a standard Magnetic Resonance Imaging (MRI) system. Because gradient coils are electromagnets operating within the strong magnetic field of the MRI system, there is a concern regarding the magnitude of net forces and torques on the coil. In particular, the possibility of coil failure within the MRI system must be considered. The purpose of this thesis is to evaluate the safety of insert gradient coil use in whole-body MRI systems.

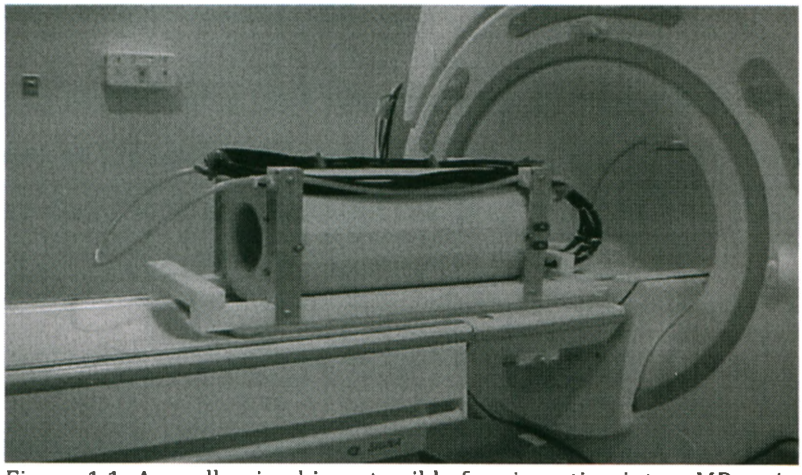

Figure 1.1: A small animal insert coil before insertion into a MR main magnet.

1.1 MRI Basics:

In an imaging sample there is a collection of spins associated with the nuclei in that sample. In the presence of an external field, the magnetic moments of these nuclei will either align parallel or anti-parallel with the main field [1]. The magnetic moment per unit volume is defined as the magnetization [1.1] of the sample.

$$\vec{M} = \frac{\vec{\mu}_{total}}{V} = \frac{\rho_o \gamma^2 h^2}{16\pi^2 kT} B_o \qquad [1.1]$$

where: $\vec{\mu}_{total}$ is the sum of the magnetic moments of the sample, ρ_o is the proton density of the sample, γ is the gyromagnetic ratio of the nuclei in question, for water γ =42.577 MHz/T, h is Plank's constant h=6.63 x 10^{-34} Js, k is the Boltzmann constant k=1.38 x 10^{-23} J/K, T is the temperature of the sample in Kelvin, K, and B_o is the external field in Tesla, T. The main field will apply a torque [1.2] on the magnetic moments of the nuclei:

$$\vec{N} = \vec{\mu} \times \vec{B} \qquad [1.2]$$

where: $\vec{N}$ is the torque on the magnetic moments, $\vec{\mu}$ is the magnetic moment of the nuclei and $\vec{B}$ is the main polarizing field.

Because of the presence of a non-zero angular momentum parallel to the magnetic moment of the nuclei, the torque applied to the magnetic moments of the nuclei will cause them to precess around the fixed axis. The rate that they rotate around the fixed axis is defined by the Larmor [1.3] equation:

$$\omega = \gamma B_o \qquad [1.3]$$

where: ω is the frequency of precession, γ is the gyromagnetic ratio of the nuclei and B_o is the magnitude of the external field in Tesla. The rate that the nuclei will precess about the fixed axis is dependant on the field strength. In MR systems, a field gradient is applied that spatially varies the main field. This will cause the nuclei to precess at different rates spatially within the magnet, resulting in a frequency dependent on position within the sample.

Magnetization is a vector quantity, its components are usually identified as longitudinal and transverse magnetization. Longitudinal magnetization relates the amount of magnetic moments, per unit volume, that are aligned with the main field. Transverse magnetization is the bulk magnetization in the plane perpendicular to the main field.

An RF magnetic field is applied which can tip the magnetic moments away from the main field. The most common RF pulse will tip the magnetic moments 90° from the *z*-axis. After the initial RF pulse of 90° all of the magnetization will be in the transverse plane, and as the longitudinal magnetization returns to the initial state, the transverse magnetization will decay according to the following:

$$M_{xy} = M_o e^{-t/T_2^*} \qquad [1.4]$$

where: M_{xy} is the magnetization in the transverse plane, M_o is the initial magnetization and T_2^* is the transverse relaxation time constant. The longitudinal

magnetization after a RF pulse of 90° will return according to the following equation:

$$M_z = M_o(1 - e^{-t/T_1}) \qquad [1.5]$$

where: M_z is the longitudinal recovery, M_o is the initial magnetization and T_1 is the longitudinal relaxation time constant, which is also dependent on the nuclei of interest. For all nuclei $T_2^* << T_1$, and so the transverse magnetization will decay at a much faster rate than the longitudinal magnetization will regrow.

1.2 MR Systems:

1.2.1 Main Magnets

In order to produce bulk magnetization within a material, a very strong external magnetic field is applied in MRI. These systems need to produce a very uniform main field over the imaging region. The inhomogeneity of a main magnet describes the amount that the field will vary over the sample to be imaged. Typical uniformity values for imaging are a few parts per million.

The basic geometric properties of a MR main magnet are the cold bore, the warm bore, the magnet windings region and the bore length. The warm bore is the open region that is accessible to the patient and contains the imaging region. The cold bore is the spatial region that includes the warm bore and the built in gradient and RF coils for the main magnet design. During the course of this study, the insert coil's position and orientation will be varied in the volume defined by the cold bore. The magnet windings region is defined by the volume in which the main magnets wires are located. The bore length is the length of the main magnet.

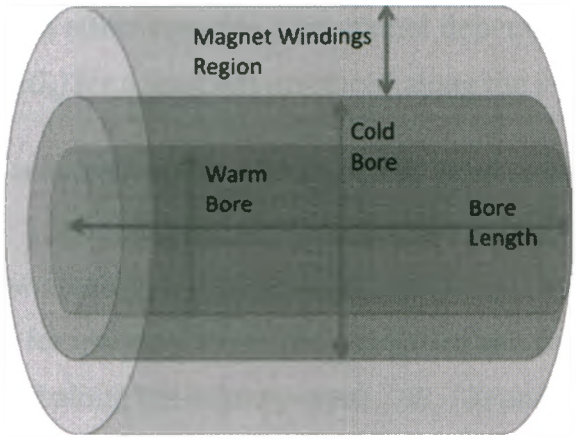

Figure 1.2: A schematic displaying the physical locations of the warm bore, cold bore, magnet windings region and the bore length

For this study, it was necessary to have a model of a main magnet that would be comparable to what is in use in the industry at that field strength. For reference, we consider the following two typical MRI systems. The Phillips Achieva® 3.0 T X-Series MRI is a 3.0 T whole body magnet system, with a 50 cm FOV and a maximum gradient strength of 80 mT/m. The Siemens Magnetom® Verio 3.0 T is a 3.0 T whole body magnet with a 70 cm diameter bore, a 50 cm FOV and a maximum gradient strength of 45 mT/m. Both magnets have a 50 cm FOV, with the differences being in the maximum gradient strength and bore diameter. The Magnetom® Verio 3.0 T was designed to have a larger bore to accommodate larger patients, while the smaller bore of the Phillips Achieva® 3.0 T X- Series allows for larger maximum gradient strengths.

1.2.2 Gradient coils

Gradient coils provide a change in the B_z component of field over a spatial region. This will cause the nuclei to precess at a different frequency based upon

their physical location, in effect creating a positional dependence on the frequency of precession: $\omega=\gamma(B_o+zG_z)$ for a gradient produced along the z-axis.

Insert coils are a subset of MR gradient coils. They are smaller and produce larger gradients over a small spatial region, thereby allowing for higher image resolution. There are two main types of coils: transverse and longitudinal coils, both of which are necessary for imaging. Transverse coils, Gx and Gy, produce changes in the B_z component of field along the x- and y- axis, $\partial B_z/\partial x$ and $\partial B_z/\partial y$ respectively. Longitudinal coils, Gz, produce a change in the B_z component of field along the z-axis, $\partial B_z/\partial z$. Gx and Gy coils are considered the same type because they share the same wire pattern, just rotated by 90° about the z-axis.

1.3 Gradient Coils: Design and Performance Parameters

The efficiency of an insert coil is defined as the gradient strength produced per unit current. For a gradient coil producing a gradient of 40 mT/m while carrying 100 A of current, the efficiency would be 0.4 mT/m/A. The gradient strength is the change in the main field produced over a spatial region, if the field varies by 25 mT over a span of 10 cm, the gradient strength would be 250 mT/m. The larger the differences in field produced over a region, the larger the differences in precession frequencies for the nuclei in that region. Typical whole-body gradient coils have efficiencies of between 0.1 and 0.2 mT/m/A. Typical insert gradient coils have much higher efficiencies between 0.5 and 2 mT/m/A.

Gradient fields must be turned on and off many times during a typical imaging sequence. The rate at which a coil can be switched on or off is determined in part by the inductance of the coil. A large inductance will limit the rise times that a gradient coil can achieve, while a small inductance allow for fast gradient switching times. The inductance of an insert coil is dependent on geometry. The inductance calculated in this study used the Neumann formula [2]:

$$L = \frac{\mu_o}{4\pi} \oint\oint \frac{ds \cdot ds'}{|r|} \qquad [1.6]$$

where: μ_o is the permeability of free space $4\pi \times 10^{-7}$ Wb/A/m, ds and ds' are two current contours that are being integrated over and $|r|$ is the distance between the contours. The calculated value is in units Henry, H. By minimizing inductance while maximizing the efficiency of the insert, imaging sequences are possible that have shorter gradient echo times that allow for imaging of biological features with shorter T_2^* while maintaining higher image resolutions. With the inductance directly proportional to the amount of wire counters in an insert coil squared, by minimizing inductance the resistance of the insert coil is also reduced. This will decrease the heating of the coil.

The vast majority of insert coils are cylindrical in geometry and this is the only geometry considered in this thesis. The size of the insert coil should be appropriate for the sample size. In order to account for the varying applications of insert coils, this study will investigate coil radii ranging from 5 cm (e.g. for mouse imaging) to 20 cm (e.g. for human head imaging). The length to diameter ratio, or aspect ratio, is the ratio of the length of the insert coil to the diameter.

When the size of an insert coil decreases, the field of view (FOV) of the insert coil will also decrease. The typical FOV is a sphere centered at the isocentre of the insert coil, but there has been several design algorithms that have differed from this approach. In the work by de Bever [3] the design of multiple imaging region coils were evaluated in order to image multiple specimens with the same sequence. In the work by Chronik [4] a head coil was designed with an off centered FOV to image the carotid arteries. In this study, only designs with FOVs centered in the coil are considered, as they are the most common.

The resistance of a coil is the main contributor to coil heating during operation. The resistivity and current carrier geometries determine the resistance of a coil. The resistivity of a material relates the change in the electric field produced for a given current density and is defined by Ohm's Law [1.7]:

$$E=\rho J \qquad [1.7]$$

where: E is the electric field produced for a given current density, J, for a material that has a resistivity ρ, copper has a resistivity of 1.72×10^{-8} Ωm at 20°C .

The resistance of a current carrier is related to the resistivity of the material by [1.8]. From this the resistance is dependant on the total length and cross sectional area of the wire. For an insert coil that has been fabricated using a constant diameter of copper wire, the total length of wire used will be the determining factor for the total resistance.

$$R = \frac{\rho L}{A} \qquad [1.8]$$

where: ρ is the resistivity of the conductor, L is the total length of wire and A is the cross sectional area of the wire.

The resistance of a current carrier has a temperature dependence [1.9].

$$R(T) = R_o[1 + \alpha(T - T_o)] \qquad [1.9]$$

where: R_o is the resistance of the conductor at the reference temperature, T_o, and α is the temperature coefficient of resistivity, which for copper is 0.00393 $(°C)^{-1}$. As the temperature of the conductor increases, so does the resistance.

Using the change in thermal energy [1.10] for a given conductor, the temperature increase of an insert coil can be determined.

$$dQ=mcdT \qquad [1.10]$$

where: dQ is the change in thermal energy of the conductor, m is the total mass, c is the specific heat, for copper c = 390 J/Kg/K, and dT is the temperature change of the conductor. The power delivered to an electric circuit is defined below by [1.11]:

$$P=I^2R \qquad [1.11]$$

where: P is the power delivered to the circuit in J/s, I is the current in the electric circuit and R is the total resistance. The power is also equal to the rate of thermal energy change, so dividing [1.10] by dt:

$$\frac{dQ}{dt} = mc\frac{dT}{dt} \qquad [1.12]$$

where: dQ/dt is the thermal energy change and dT/dt is the rate of temperature in the current carrier. Making the substitution that $P=dQ/dt$ into [1.12] and isolating the rate of temperature change, while substitution [1.10] for the resistance:

$$\frac{dT}{dt} = \frac{I^2R(T)}{mc} = \frac{I^2R_o(1+\alpha(T-T_o))}{mc} \qquad [1.13]$$

The resistance of a conductor's dependency on temperature has the effect that if an insert coil is not sufficiently cooled and the temperature is allowed to increase, it will be a compounding effect and increase the temperature more rapidly.

1.4 Numerical Calculations:

In the course of this project under different situations, the Lorentz force and torque on the insert coil in a MR main magnet will be calculated and evaluated to determine the safety of the insert coil. The methods for achieving this are described in the following paragraphs.

1.4.1 The Biot-Savart Law:

The integral form of the Biot-Savart Law [1.14] is the starting equation used for magnetic field calculations and by simplifications the integral form is reduced to an equation that is better suited for numerical computations.

$$\vec{B}(\vec{r}) = \frac{\mu_o}{4\pi}\iiint_V \frac{\vec{J}(\vec{r}')\times(\vec{r}-\vec{r}')}{|\vec{r}-\vec{r}'|^3}d\vec{V} \qquad [1.14]$$

If we approximate a continuous current density as a finite current flowing through an infinitely thin wire:

$$J(\vec{r}')dV' \Rightarrow Id\vec{l}(\vec{r}') \qquad [1.15]$$

where: $d\vec{l}(\vec{r}') = \hat{i}dl_{x'} + \hat{j}dl_{y'} + \hat{k}dl_{z'}$

Substituting into [1.14]:

$$\vec{B}(\vec{r}) = \frac{\mu_o}{4\pi}\oint \frac{I(\vec{r}')d\vec{l}(\vec{r}') \times (\vec{r} - \vec{r}')}{|\vec{r} - \vec{r}'|^3} \qquad [1.16]$$

If the current is constant and the same at every point along the wire, then $I(\underline{r}')$ becomes I and [1.16] becomes:

$$\vec{B}(\vec{r}) = \frac{\mu_o I}{4\pi}\oint \frac{d\vec{l}(\vec{r}') \times (\vec{r} - \vec{r}')}{|\vec{r} - \vec{r}'|^3} \qquad [1.17]$$

If we want to consider the net magnetic field at a location as due to the sum of infinitesimal contributions:

$$d\vec{B}(\vec{r}) = \frac{\mu_o I}{4\pi}\frac{d\vec{l}(\vec{r}') \times (\vec{r} - \vec{r}')}{|\vec{r} - \vec{r}'|^3} \qquad [1.18]$$

The problem then becomes:

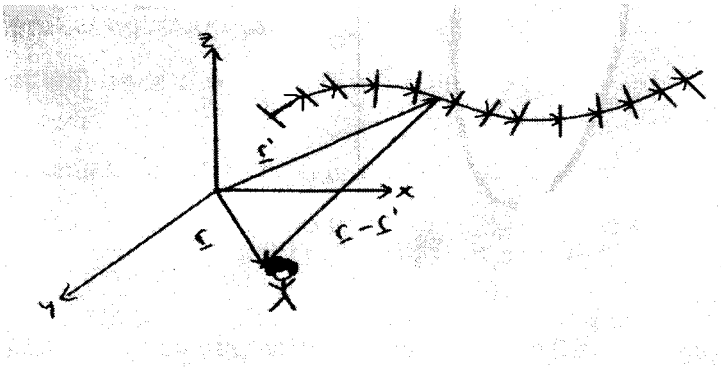

Figure 1.3: Depicts the relationship of the distance relationships used in the numerical calculations of the Biot-Savart Law. The vector $\underline{r}'$ is from the origin to an element and the vector $\underline{r}$ is from the origin to the point where the magnetic field is calculated, so the vector subtraction $\underline{r}$ - $\underline{r}'$ relates the vector from the element in the current carrying wire to the point where the magnetic field is calculated.

Figure 1.3 shows the vector notation used in the calculation of the magnetic field due to one section of wire. If the net magnetic field due to all of the wire contributions is to be evaluated then the sum of all the parts is needed and this motivates the discrete from of the Biot-Savart Law that will be used to evaluate the magnetic field later:

$$\vec{B}(\vec{r}) = \frac{\mu_o I}{4\pi} \sum_{i=1}^{N} \frac{d\vec{l}(\vec{r}') \times (\vec{r} - \vec{r}')}{|\vec{r} - \vec{r}'|^3} \qquad [1.19]$$

for N elements in a wire pattern.

1.4.2 Lorentz Force:

When two current carrying wires become sufficiently close they each will experience a Lorentz Force. This force will be experienced by every part of the wire pattern and so if a discrete method is used then the net force is the vector sum of the force on each wire element. In a similar manner to the evaluation of the Biot-Savart

Law, the Lorentz equation for force on a current carrying wire will be reduced to a manner that will be computationally simple.

Following is the analytical Lorentz force equation:

$$\vec{F} = (nqv_d A)\int (\vec{l} \times \vec{B}) d^3x \qquad [1.20]$$

Where: n is the number of charge carriers in the wire, q is the charge on the carriers, v_d is the drift velocity, A is the cross sectional area, l is the vector relating change in the wire pattern and $\vec{B}$ is the magnetic field produced by the other electromagnet.

Taking the current density to be: $J=nqv_d$, then [1.20] becomes:

$$\vec{F} = (JA)\int (\vec{l} \times \vec{B}) d^3x \qquad [1.21]$$

the product JA is just the total current in the wire, I. Making this substitution [1.21] becomes:

$$\vec{F} = I\int (\vec{l} \times \vec{B}) d^3x \qquad [1.22]$$

This is the net force on the wire, the force on an infinitesimal section of wire is:

$$d\vec{F} = I(d\vec{l} \times \vec{B}) \qquad [1.23]$$

To compute the net force on the wire the individual contributions on each section of wire is summed to yield the form used to calculate the net force on a current carrying wire pattern:

$$\vec{F} = I\sum_{i=1}^{N} (d\vec{l}_i \times \vec{B}_i) \qquad [1.24]$$

Where: I is the current in the wire, $d\vec{l}_i$ is one section of wire and $\vec{B}_i$ is the magnetic field produced by the external electromagnet at $d\vec{l}_i$. This equation assumes that there are N elements of wire in the wire segment.

1.4.3 Torque:

A current carrying wire in a magnetic field experiences a force and a current carrying wire that experiences a force may also experience a torque [1.25].

$$\vec{\tau} = \vec{r} \times \vec{F} \qquad [1.25]$$

Where: $\vec{r}$ is the vector from the axis of rotation to the location of applied force and $\vec{F}$ is the force being applied.

For the purposes of this thesis, the force applied is obviously the Lorentz force and now substituting [1.22] into [1.25] results in:

$$\vec{\tau} = I(\vec{r} \times \int (\vec{l} \times \vec{B}) d^3x) \qquad [1.26]$$

If only the torque due to the force on one element of wire is considered:

$$d\vec{\tau} = I(\vec{r} \times (d\vec{l} \times \vec{B})) \qquad [1.27]$$

This is the torque on one element of wire, the net torque over the entire wire pattern is the sum of the torque on each segment of wire:

$$\vec{\tau} = I\sum_{i=1}^{N} (\vec{r}_i \times (d\vec{l}_i \times \vec{B}_i)) \qquad [1.28]$$

Where: I is the current in the wire pattern, $\vec{r}_i$ is the vector from the axis of rotation to the infinitesimal section of wire, $d\vec{l}_i$ relates how that wire segment is changing and $\vec{B}_i$ is the magnetic field produced by the external source at the wire segment. This assumes that there are N sections in the wire pattern. This is the equation that will be used to evaluate torque in later computations.

1.4.4 Discretization:

The process of dividing a wire pattern into smaller, simpler computationally regions is known as discretization. These regions must retain the original wires position and relate how the wire is changing at a given position. When dealing with current carrying conductors the current flowing in the wire section is also needed. These three concerns need the representation to contain a position, (x, y, z), the change in the wire pattern,(dx, dy, dz), and the current I. This information can be tabulated in a matrix using the following format:

$$\begin{bmatrix} x_1 & x_2 & \dots & x_n \\ y_1 & y_2 & \dots & y_n \\ z_1 & z_2 & \dots & z_n \\ dx_1 & dx_1 & \dots & dx_1 \\ dy_1 & dy_2 & \dots & dy_n \\ dz_1 & dz_2 & \dots & dz_n \\ I_1 & I_2 & \dots & I_n \end{bmatrix} \qquad [1.29]$$

This representation has two benefits: 1) the order of column vectors does not effect any final calculation and 2) the current in an individual wire segment can be isolated and varied.

The number of divisions used to represent an object is key to the accuracy of the representation. Figures 1.4a -1.4d are different discrete approaches to representing a circle. As the number of divisions used in the loop increase the approximation improves. The trade off is that as the number of divisions in the loop increases the speed of calculation decreases with an increase in numerical error due to the increased number of calculations.

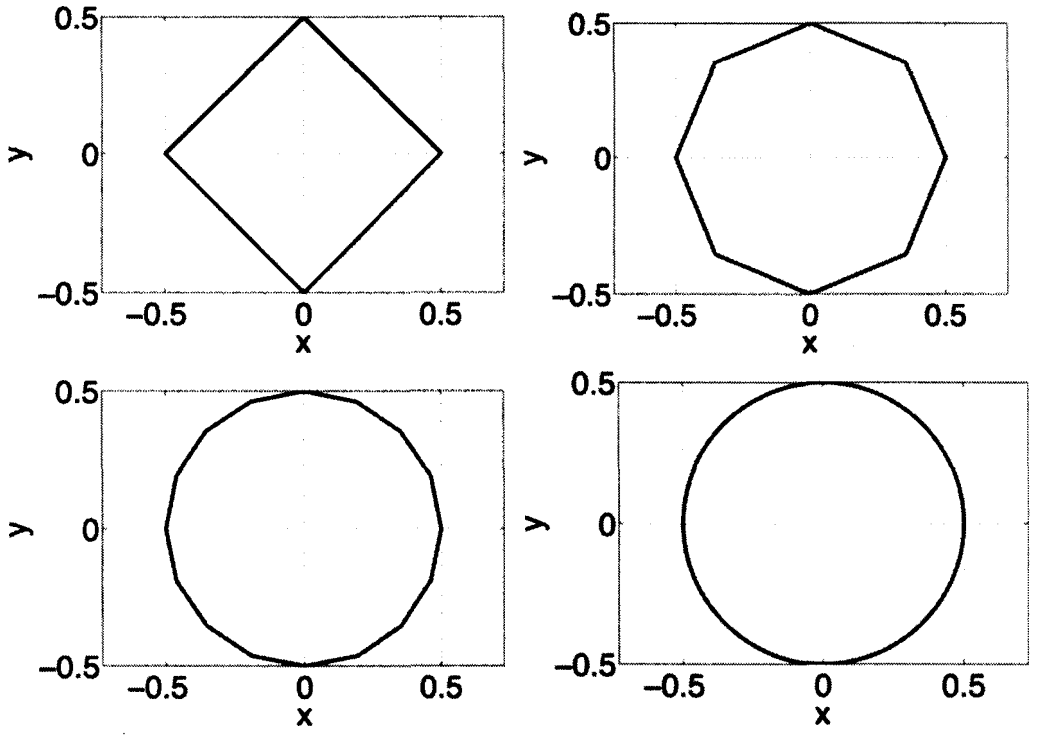

Figures 1.4a -1.4d: counter clockwise from upper left: Each plot is an approximation to a circle, with a radius of 0.5 m, with Figure 1.4a having 4 divisions, Figure 1.4b having 8, Figure 1.4c having 16 and in Figure 1.4d the loop is approximated by 100 divisions. Note that with only 4 divisions the circular approximation is actually a square and as the number of elements in the approximation increases the final results appears more continuous.

1.5 Insert Coil Failures

An insert coil is considered to have failed when the coil has deviated from the original design in a significant manner. This can happen in many different ways, but there are two main types of insert coil failures; mechanical and electrical failures. A mechanical failure is when the structural design of the insert coil fails. This can happen when the internal stresses in the coil are larger than the structural supports and the insert coil physically breaks. Another mechanical failure is when the insert coil is not properly cooled, or the cooling mechanism breaks down, so that the coil heats up to the point that it is no longer operable. Mechanical failures are coil fabrication concerns, and will not be discussed further in this project.

Electrical failures are when the current in the insert coil deviates from the desired path resulting in a coil short or an open. An open occurs when there is a break in the circuit, not allowing any current to flow in the insert coil. A short occurs when return wires make contact with a wire section, creating a short that allows for the current to by-pass entire sections of the insert coil. When calculating the Lorentz force and torque on the insert coil, this type is the most important. During the course of this project, different electrical failures will be investigated to determine safe regions for coil operation.

In order to prevent mechanical failures of an insert coil, the wire pattern is typically milled into a plastic former to add structural stability. The wire is then inserted into the milled pathways and set into place with epoxy. If it is determined that the coil needs forced cooling measures, than cooling pipes, typically containing chilled water, are milled into paths beside the current windings so that they can provide conductive cooling. Depending on the size of the insert coil, air-cooling can be sufficient to maintain the coil temperature at operable levels.

Care is taken when winding gradient coils so that wires do not touch. After long-term usage, the mechanical vibrations and heating may deteriorate the coil structure such that wires may come into contact within the coil. This results in a major coil failure. During the course of this project, the worst case electrical failures will be investigated to determine what precautions, if any, are needed to ensure that the Lorentz force and torque on the insert coil will not cause the insert coil to move.

1.6 Thesis Overview:

With the final goal of this study to determine the safety of small animal insert coils in their implementation in MR main magnets, the final result should indicate the locations where the insert coil can be considered safe. With a maximum allowable net force and net torque, the safety of an

insert coil can be determined for each rotation, location and operation mode considered.

A main magnet representation was chosen from a literature review, and evaluated for accuracy versus a simplified representation of that same magnet. The simplified version was created in order to increase the speed with which the force and torque calculations could be conducted.

Eight different gradient coils are considered in this thesis: 4 transverse coils with varying radii, and 4 longitudinal coils with the same varying radii. Each coil was translated to different locations with respect to the main magnet model, and net forces and torques were evaluated as a function of failure mode. From this work, the safety of coil operation could be evaluated under a wide variety of operational conditions that may occur during insert gradient coil usage.

A Safe Region was defined which represents the centre of mass locations, that for any operation mode and rotation, the net forces and net torques on the insert coil are considered not large enough to cause coil motion. This is done by only plotting locations that are under the thresholds for every operation mode for each mis-position and orientation considered. The final result is the identification of a region with respect to the main magnet that is of primary concern when evaluating coil safety, regardless of coil size, orientation, and failure mode.

References:

[1]: Haacke, Mark E., Brown, Robert W., Thompson, Michael R., Vankatesan, Ramesh (1999). *Magnetic Resonance Imaging- Physical Principles and Sequence Design.* Toronto: Wiley-Liss

[2]: Grover, Frederick W. (1962). *Inductance Calculations; Working Formulas and Tables.* New York: Dover Publications Inc.

[3]: De Bever, Joshua T. (2007). *Multiple-Imaging-Region Gradient Coil Insert for Parallel Imaging of Mice in MRI.* Unpublished masters dissertation, University of Western Ontario, Canada.

[4]: Chronik, Blaine A., Alejski, Andrew, Rutt, Brian K. (2000). Design and Fabrication of a Three-Axis Edge ROU Head and Neck Gradient Coil. *Magnetic Resonance in Medicine, 44,* 955-963

[5]: "Phillips Healthcare". Achieva 3.0T X-series MRI. http://www.healthcare.philips.com/main/products/mri/systems/achieva3t/index.wpd (July 23, 2009)

[6]: " Siemens Medical". MAGNETOM Verio 3T. http://www.medical.siemens.com/webapp/wcs/stores/servlet/ProductDisplay~q_catalogId~e_-11~a_catTree~e_100001,12786,12754,14330~a_langId~e_-11~a_productId~e_181442~a_storeId~e_10001.htm (July 23, 2009)

[7]: Chronik, Blaine A. et al (1998). Constrained Length Minimum Inductance Gradient Coil Design. *Magnetic Resonance in Medicine, 39,* 270-278.

[8]: Turner, Robert (1993). Gradient Coil Design: A review of Methods. *Magnetic Resonance Imaging, 11,* 903-920

[9]: Turner, R (1988). Minimum Inductance Coils. *Journal of Physics [E], 21,* 948-952

[10]: Alsop, David C., Connick, Thomas J. (1996). Optimization of Torque-Balanced Asymmetric Head Gradient Coils. *Magnetic Resonance in Medicine, 35,* 875-886

[11]: " Molecular Expressions". Electricity and Magnetism Introduction. http://micro.magnet.fsu.edu/electromag/electricity/inductance.html (July 28, 2009)

[12]:Cheng, Yu-Chun N. et al (2004). A Comparison of Two Design Methods for MRI Magnets. *IEEE Transactions on Applied Superconductivity, 14*(3), 2008-2014

[13]:"Epoxies.com". 50-3100 High Thermal K Heat Transfer Epoxy Resin. http://www.epoxies.com/therm.htm (Aug 13/09)

[14]: "Wikipedia". Tensile Strength. http://en.wikipedia.org/wiki/Tensile_strength (Aug 13/09)

Chapter 2: METHODS

Through this next section the processes and ideas needed to evaluate a Safe Region will be presented. This will involve discussing the main magnet and gradient coil representations, the manner that translations and rotations of the insert coil will be instigated, the determination of the locations that the insert coil will be translated to, the insert coil failure modes, implementation of a failure mode, the algorithm used to calculate the force for each position and rotation, the Safe Region thresholds and the determination of the Safe Region - Force, Safe Region - Torque and the intersection of them both in the final Safe Region.

2.1 Main Magnet Representation:

The insert coils and main magnet were represented by discrete wire segments as detailed in section 1.4.4. The information needed for any calculations were stored in a matrix detailed by [1.29].

2.1.1 Literature Search for a 1.0 T main magnet:

From a literature search a design of a 1 T main magnet with a cold bore measuring 1 m in diameter and with a length of 1 m was found [1]. The article details 4 magnet designs, all with similar performance characteristics. The magnet detailed in table I was chosen to represent the main magnet of our system because the physical parameters were a close match to a physical system. With the difficulties in finding the schematics for a main magnet design, the magnets in this paper were selected as the best available fit for a realistic design. The selected magnet has a theoretical inhomogeneity of 2 ppm inside a DSV of 30cm. The dimensions of the system were found using the wire dimensions of 1mm x 1mm and the number of radial and axial windings detailed in the article. In the article it was assumed that current flowed through the centre of the wire, and this assumption was maintained when discretizing the coils for the purpose of this study.

	N_ρ	N_z	ρ_{min} (m)	ρ_{max} (m)	z_{min} (m)	z_{max} (m)
coil 1	16	10	0.521	0.536	0.011	0.020
coil 2	10	16	0.528	0.538	0.227	0.242
coil 3	59	54	0.521	0.579	0.362	0.415
coil 4	156	114	0.723	0.878	0.382	0.495
coil 5	56	109	1.280	1.335	0.006	0.114

Table 2.1: displays the parameters for each current carrying solenoid that comprises the main magnet design. This is an amendment of table 1 presented by Cheng[1]. This table details the coils for z>0, since the magnet is symmetric about z=0 the coils for z<0 are the negative of the z values presented here while maintaining the radial and current parameters. The smallest and largest radial windings are given by ρ_{min} and ρ_{max} respectively and the closest winding to the z = 0 m was given as z_{min} with the furthest winding being z_{max}. The number of radial and axial windings in a solenoid were given as N_ρ and N_z respectively and each winding carried 110 A of current.

2.1.2 Simplified Main Magnet:

In order to speed up calculations another magnet representation was presented that maintained the geometric properties and current densities presented in table 2.1 but reduced the number of radial and axial windings. The radial windings were placed at the minimum, maximum and midpoints of the radial ranges for their respective coils detailed in table 2.1. The axial windings separation was at most 5% of the inner radius of that respective coil. The current in each wire for a given coil was found by dividing the total current in that coil by the total number of windings in the coil.

	N_ρ	N_z	ρ_{min} (m)	ρ_{max} (m)	z_{min}(m)	z_{max} (m)	I_w (A)
coil 1	3	3	0.521	0.536	0.011	0.020	1960
coil 2	3	3	0.528	0.538	0.227	0.242	-1960
coil 3	3	5	0.521	0.579	0.362	0.415	-23364
coil 4	3	5	0.723	0.878	0.382	0.495	130416
coil 5	3	3	1.280	1.335	0.006	0.114	-74604

Table 2.2: The parameters for the simplified main magnet. The additional column displays the current flowing through each wire, in their respective coil, needed to maintain the current density. The parameters listed are the same as in table 2.1, but with the addition of I_w (A) that lists the current carried in one winding of the simplified solenoids.

2.1.3 Error Analysis for the Simplified Main Magnet:

To estimate the error introduced by simplifying the design presented by Cheng [1], the magnetic field was calculated at 20 000 points for both magnet designs. These points were selected to be in the region defined by: -0.3 m < x < 0.3 m, -0.3 m < y < 0.3 m and -1 < z < 1 m. This region was selected because the magnetic field calculations needed to determine the force and torque on the insert coil would be evaluated within these boundaries. The time needed to calculate the magnetic field at all 20 000 points was recorded for both magnet designs. The standard error, maximum error, mean error and mean absolute error were evaluated to determine the differences in field produced by the simplified main magnet compared to the detailed main magnet.

2.2 Gradient Coils:

The transverse insert coils in this study were selected to have radii of 5 cm, 10 cm, 15 cm and 20 cm, with a length to diameter ratio, or aspect ratio, of 2. These radii were selected to represent the range of application of insert coils. The smaller 5 cm radii coils would be used for mouse imaging, and as the radii increases so would the specimen. The 20 cm coil would be used for human extremity imaging. An AR of two was selected to represent typical insert coil ratios. The longitudinal insert coils had the same radii, and were chosen to have an aspect ratio of less than 2. With the CCMI [2] method an exact aspect ratio is difficult to attain, so an aspect ratio that is close to 2 was considered adequate to keep the geometries of the transverse coils and longitudinal coils the same.

The number of windings used to approximate the current density for each coil was scaled such that each coil had an approximate inductance of 200 μH. With the inductance of an insert coil proportional to the number of wire contours squared, an exact inductance of 200 μH was not achievable as only whole wire contours were considered for gradient coil designs. It was decided that an

inductance close to 200 μH was acceptable for a coil design. An inductance of 200 μH was chosen to reduce the number of windings in each insert coil, and decrease the computation time as a result.

The Stream Function method [3] was used to produce the transverse gradient coils. The numbers of wire contours were 112, 80, 72 and 60 for the 5 cm, 10 cm, 15 cm and 20 cm radii coils respectively and each contour was divided into 20 wire segments. The CCMI method [2] was used to determine the Gz wire patterns.

2.3 Gradient Positioning Relative to the Main Magnet:

2.3.1 Translations:

The gradient coil was translated by adding displacements to the position elements in its discrete matrix representation. Displacements in the *x*-direction were added to the first row, *y*-direction the second row and in the *z*-direction to the third row as shown below.

$$\begin{bmatrix} x_1 + x' & x_2 + x' & x_i + x' & x_n + x' \\ y_1 + y' & y_2 + y' & y_i + y' & y_n + y' \\ z_1 + z' & z_2 + z' & z_i + z' & z_n + z' \\ dx_1 & dx_2 & dx_i & dx_n \\ dy_1 & dy_2 & dy_i & dy_n \\ dz_1 & dz_2 & dz_i & dz_n \\ I_1 & I_2 & I_i & I_n \end{bmatrix} \qquad [2.1]$$

2.3.2 Rotations:

The gradient coils position elements, (x, y, z), and the elements relating the changes in the wire, (dx, dy, dz), were rotated at each translation location. With only rotations about the *x*-axis being considered, the following is the rotation matrix, λ [2.2], used when evaluating the rotations.

$$\lambda = \begin{bmatrix} 1 & 0 & 0 \\ 0 & \cos\theta & \sin\theta \\ 0 & -\sin\theta & \cos\theta \end{bmatrix} \quad [2.2]$$

A position matrix, *R*, was formed containing the first three rows of the elements array representing the gradient coil, and a matrix was formed from rows 4-6 of the elements array containing how each wire segment is changing, *dR*. Using block matrix representation, the rotation matrix was left multiplied to both the position matrix and the derivative matrix such that the new elements array, *R'* is:

$$R' = \begin{bmatrix} \lambda \\ \lambda \\ 0 \end{bmatrix} \times \begin{bmatrix} R \\ dR \\ I \end{bmatrix} \quad [2.3]$$

2.3.3 Gradient Coil Positioning Restrictions:

The gradient coils positions were restricted to only realistic coil placements. The cold bore, radius of 50 cm and a length of 100 cm, was chosen as the physical limits of the main magnet while the wire positions were chosen as the physical limits for all gradient coils under investigation. The translation locations were chosen to outline a rectangular prism through the main magnet. Due to the cylindrical geometry of the insert coils and the main magnet, it was easier to use cylindrical coordinates to find translation restrictions and then convert them to Cartesian coordinates.

The main magnet and the gradient coils were cylindrical in shape, so the largest displacement a gradient coil, aligned parallel to the main magnet, can be translated by was $r = r_m - r_c$; where r_m is the cold bore radius and r_c is the radius of the desired gradient coil. After the gradient coil has been rotated, an effective radius, r_e, was calculated that was more accurate in restricting the gradient coils position as detailed in Figure 2.1. With the maximum radial displacement

determined the maximum x and y translations were found using simple geometry. For a square cross section the maximum radial displacement was for $x = y$. Using Pythagorean's theorem $r^2=x^2+ y^2$, for $x = y$ this leads to $x = y = r/\sqrt{2} = (r_m - r_e) /\sqrt{2}$. The parameter space detailing the rotations and translations was selected and detailed in Table 2.3.

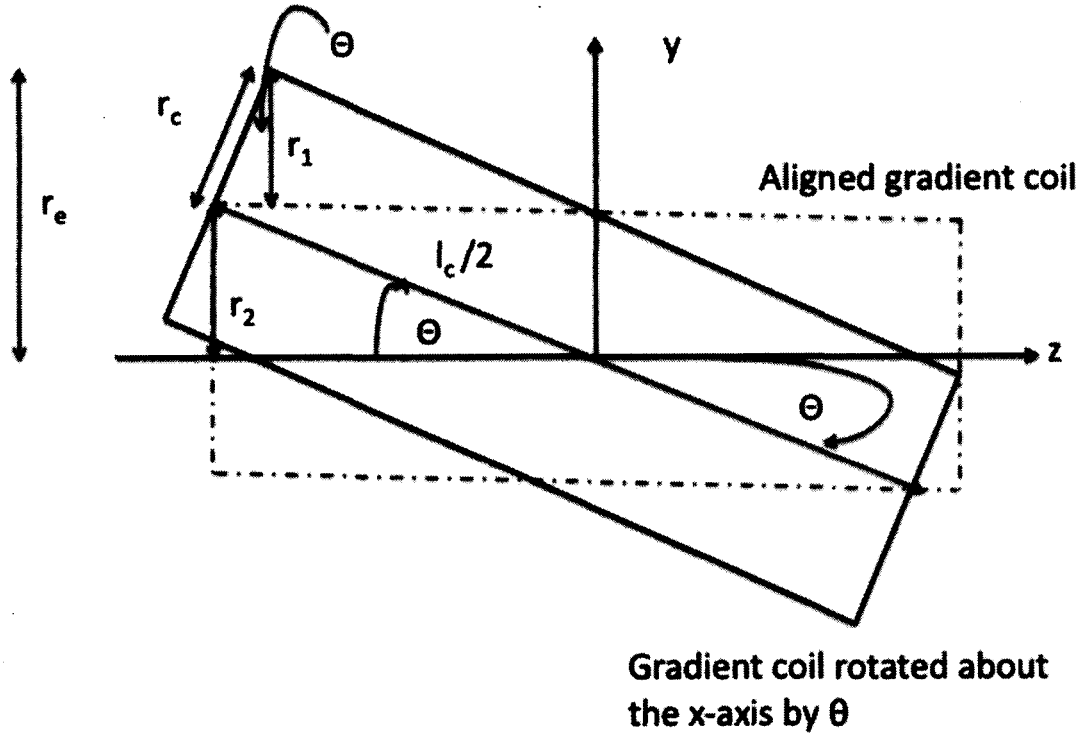

Figure 2.1: Displays an insert coil that has been rotated about the x-axis by an angle θ. The effective radius, r_e, was the sum of $r_1 + r_2$. Using trigonometry $r_1 = (l_c /2)\sin\theta$, $r_2= r_c \cos\theta$ and so $r_e = (l_c /2)\sin\theta + r_c \cos\theta$. Where l_c is the length of the gradient coil, r_c is the coil radius and θ is the angle of rotation about the x-axis. The new expression for maximum radial translation of the gradient coil is $r = r_m - (l_c /2)\sin\theta - r_c \cos\theta$.

Radii/ Parameter	5 cm	10 cm	15 cm	20 cm
x_{span}	[-20 cm, 20 cm]	[-15 cm, 15 cm]	[-10 cm, 10cm]	[-5 cm, 5 cm]
dx	5 cm	3.75 cm	2.5 cm	1.25 cm
y_{span}	[-20 cm, 20 cm]	[-15 cm, 15 cm]	[-10 cm, 10cm]	[-5 cm, 5 cm]
dy	5 cm	3.75 cm	2.5 cm	1.25 cm
z_{span}	[-100 cm, 100 cm]	[-100 cm, 100 cm]	[-100 cm, 100 cm]	[-100 cm, 100 cm]
dz	10 cm	10 cm	10 cm	10 cm
angle of rotation	-23°, -11.5°, 0°, 11.5°, 23°	-23°, -11.5°, 0°, 11.5°, 23°	-23°, -11.5°, 0°, 11.5°, 23°	-23°, -11.5°, 0°, 11.5°, 23°

Table 2.3: The ranges that the gradient coils were translated by, and the rotation about the *x*-axis for each translation. The x_{span}, y_{span}, and z_{span} define the ranges that the insert coil was translated along for the *x*- , *y*- and *z*-axis respectively. The step sizes, dx, dy and dz, for the *x*- , *y*- and *z*-axis respectively were consistent for given coil radii.

2.4 Failure Modes:

Operation modes of the insert coils were to be considered as different permutations that the current could flow in a coil to simulate different electrical failures. The current in each quadrant had two options; full short, 0 A, or normal operation, 1 A. For a coil with 4 distinct quadrants, with these two possible options for current, there were 16 possible operation modes. Current was restricted to flow in one direction only, and only full shorts were considered as failure modes.

2.4.1 Failure Modes For Transverse Gradient Coils:

Only the magnitude of force and torque were necessary to determine the Safe Regions, and so symmetry was used to reduce the number of operation modes considered. For a given Gy coil, each of the four quadrant fingerprints are identical in geometry, so ideally the force on each quadrant should be the same given that they are in the same magnetic field. With this in mind the 16 possible operation modes for a 4 quadrant Gy coil were reduced to 6. They are shown in the following figures.

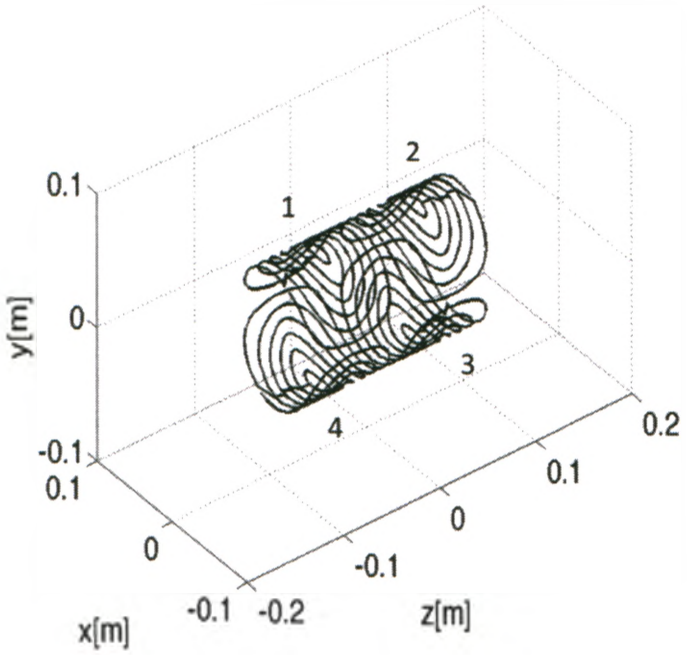

Figure 2.2: A completely functioning 5 cm radius Gy coil. The 4 fingerprint quadrants are labeled, known as the normal operation mode.

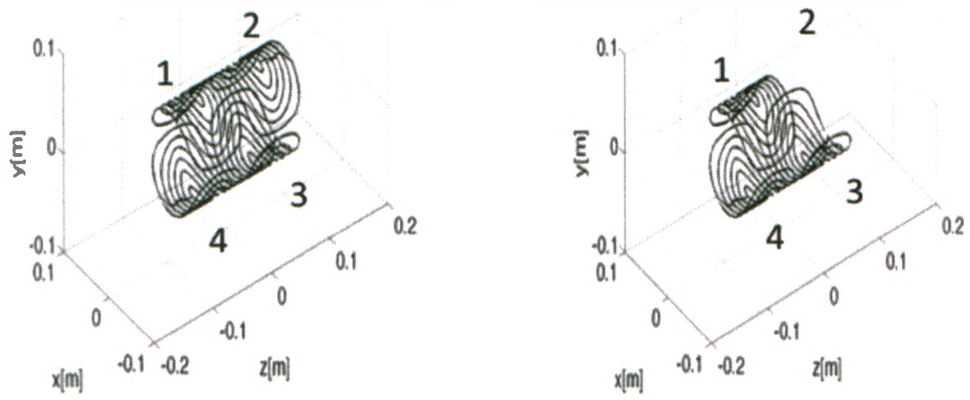

Figure 2.3: On the left is the functioning coil, the coil on the right is the first operation mode and has had a short simulated in the 2nd quadrant, $y > 0$ and $z > 0$.

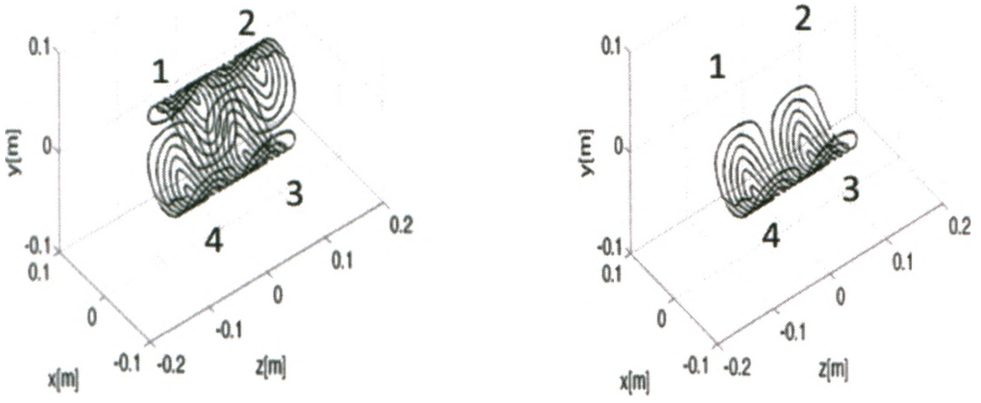

Figure 2.4: On the left is the functioning coil, the coil on the right is the fifth operation mode and has had a short simulated in the 1st and 2nd quadrant, y > 0.

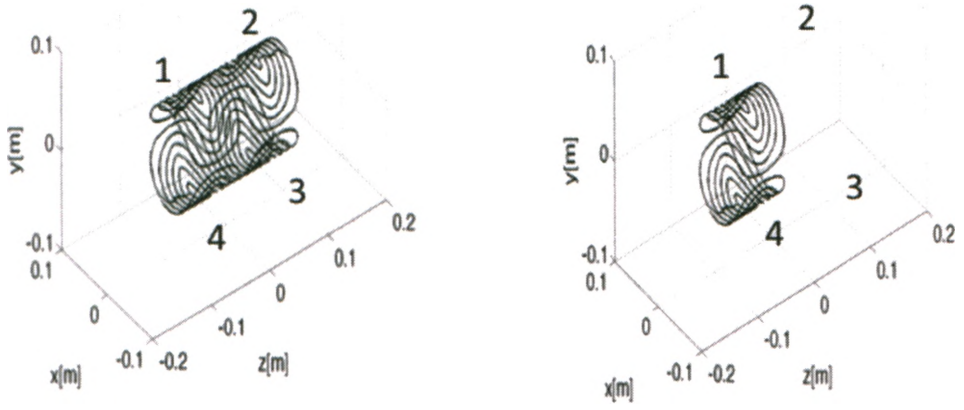

Figure 2.5: On the left is the functioning coil, the coil on the right is the sixth operation mode and has had a short simulated in the 2nd and 3rd quadrant, z > 0.

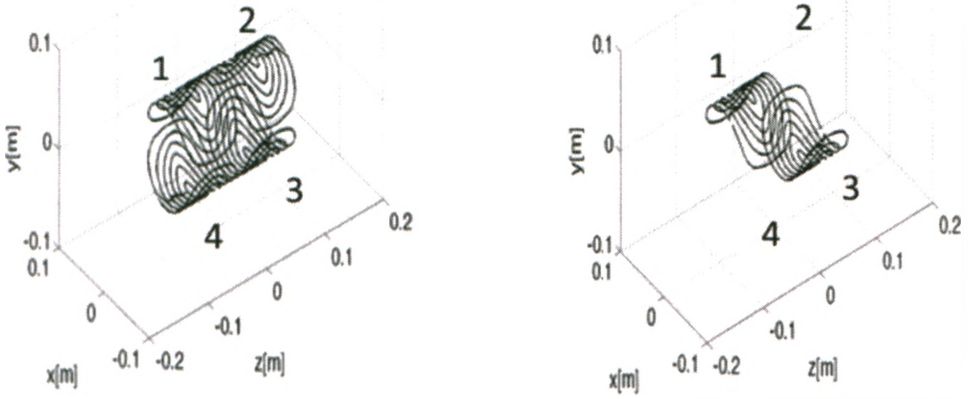

Figure 2.6: On the left is the functioning coil, the coil on the right is the seventh operation mode and has had a short simulated in the 2nd and 4th quadrant, $y > 0$ with $z > 0$ and $y < 0$ with $z < 0$.

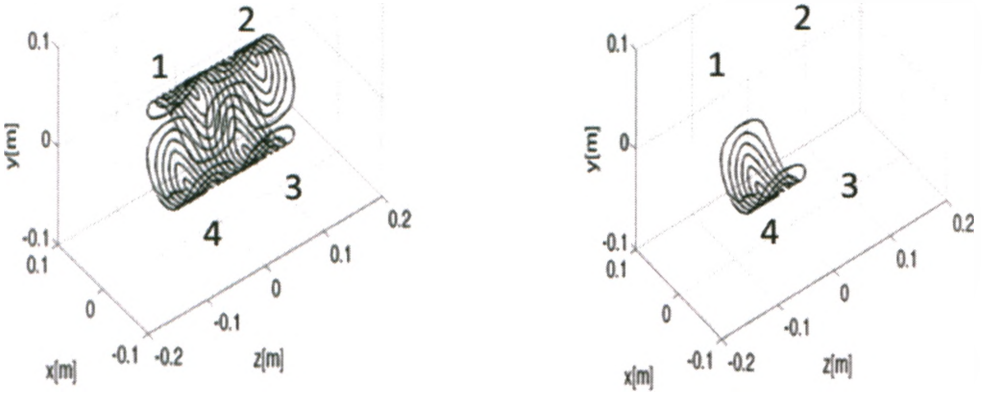

Figure 2.7: On the left is the functioning coil, the coil on the right is the eighth operation mode and has had a short simulated in the 1st, 2nd and 3rd quadrant, $y > 0$ and $y < 0$ with $z > 0$.

2.4.2 Failure Modes for Longitudinal Gradient Coils:

The process of determining operation modes was repeated for Gz coils. For the Gz coils with a radius of 5 cm and 10 cm there were 4 distinct current carrying regions leading to 16 operation modes. Using symmetry the number of operation modes simulated for these Gz coils were reduced to 9. For the Gz coils with a radii of 15 cm and 20 cm there were 2 distinct current carrying regions resulting in 4 operation modes. Using symmetry the number of operation modes for these coils was reduced to 2. These added features, quadrants 2 and 3, are what complicated the wire pattern, so that the numbers of operation modes were only reduced to 9 and not 6 like the case of the Gy coils.

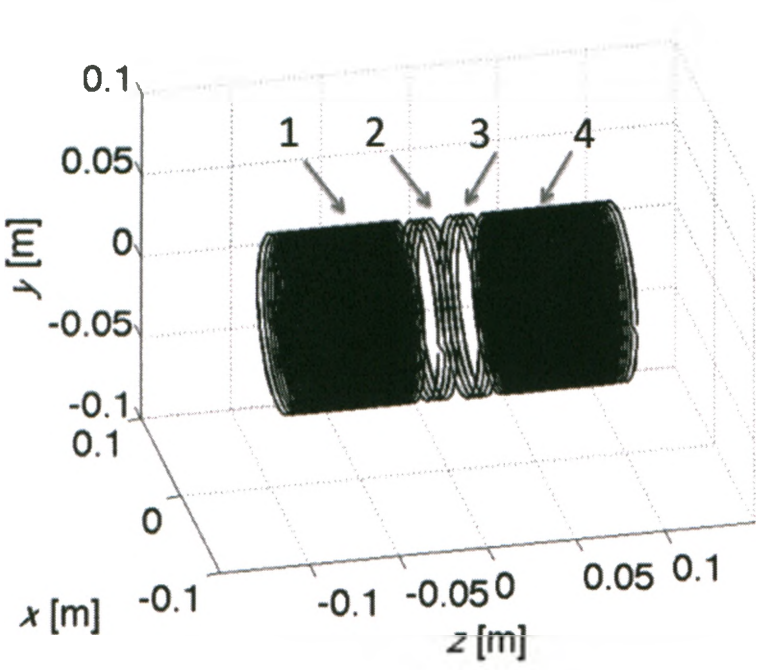

Figure 2.8: The fully functioning 5 cm radius Gz coil with the 4 current carrying regions labeled. The 10 cm radius Gz coil showed the same trends for current allocation, but for different geometric regions.

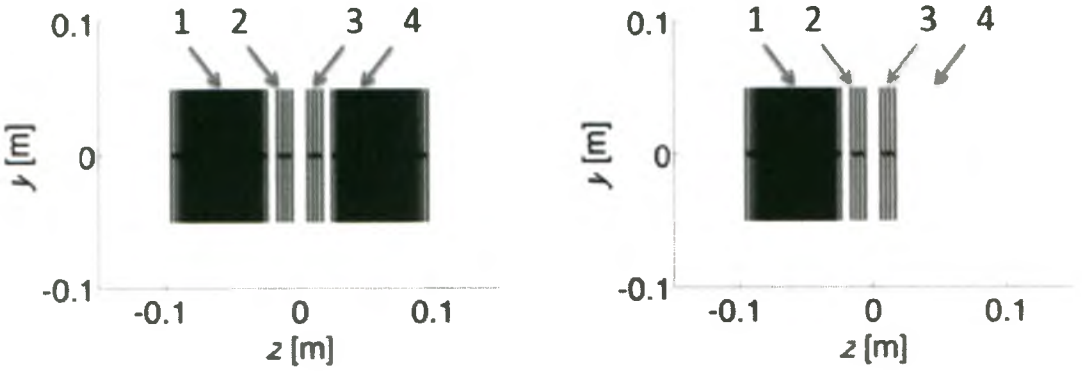

Figure 2.9: On the left is a fully functioning 5 cm radius Gz coil, on the right is the second operation mode that has had a short simulated in the 4th quadrant, z > 0.02 for the 5 cm coil and z > 0.05 for the 10 cm coil.

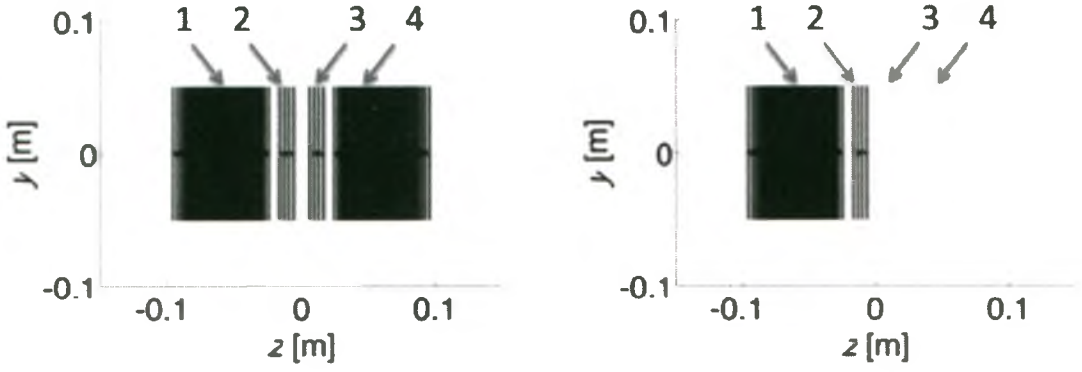

Figure 2.10: On the left is a fully functioning 5 cm radius Gz coil, on the right is the third operation mode that has had a short simulated in the 3rd and 4th quadrant, z >0 for the 5 cm coil and z >0 for the 10 cm coil.

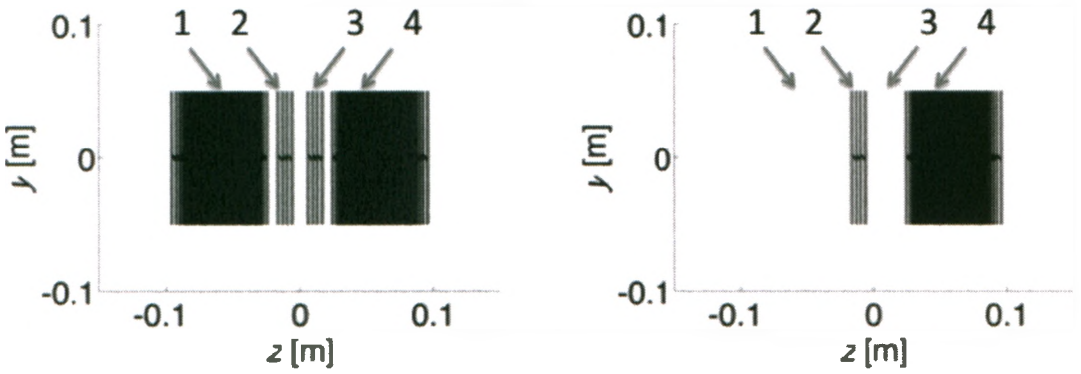

Figure 2.11: On the left is a fully functioning 5 cm radius Gz coil, on the right is the fourth operation mode that has had a short simulated in the 1st and 3rd quadrant, $z < -0.02$ and $0 < z < 0.02$ for the 5 cm coil and $z < -0.05$ and $0 < z < 0.05$ for the 10 cm coil.

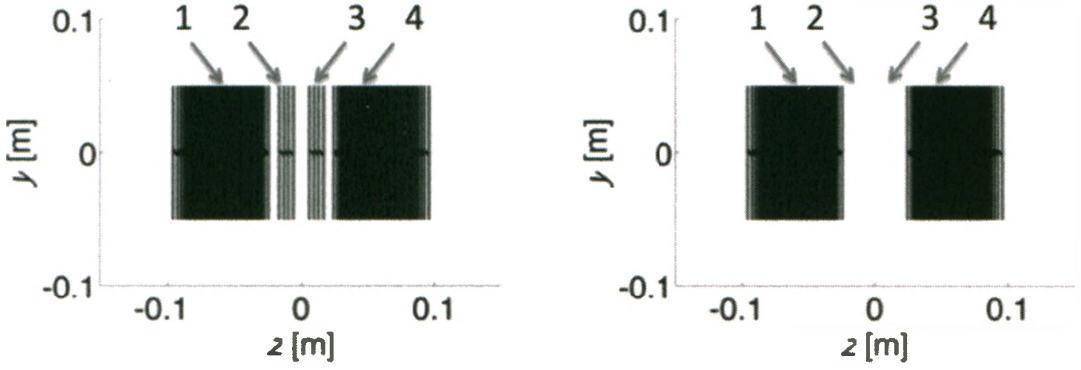

Figure 2.12: On the left is a fully functioning 5 cm radius Gz coil, on the right is the fifth operation mode that has had a short simulated in the 2nd and 3rd quadrant, $-0.02 < z < 0.02$ for the 5 cm coil and $-0.05 < z < 0.05$ for the 10 cm coil.

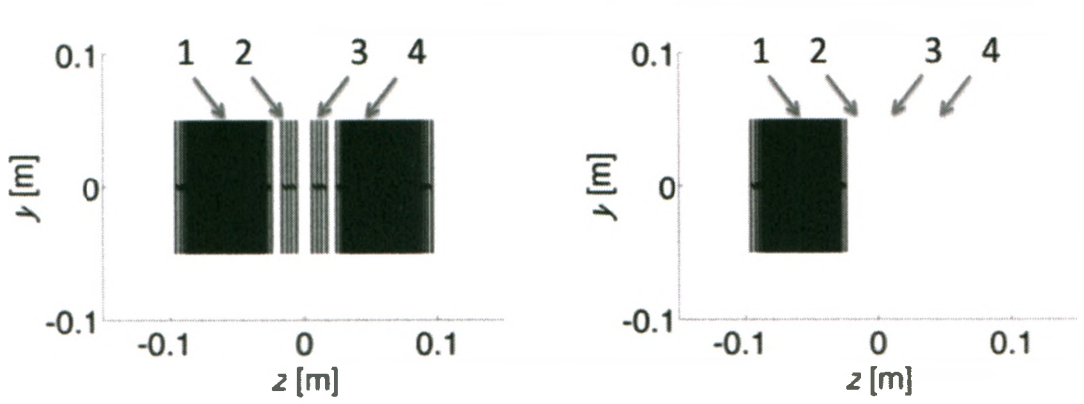

Figure 2.13: On the left is a fully functioning 5 cm radius Gz coil, on the right is the sixth operation mode that has had a short simulated in the 2nd, 3rd and 4th quadrant, z > -0.02 for the 5 cm coil and z > -0.05 for the 10 cm coil.

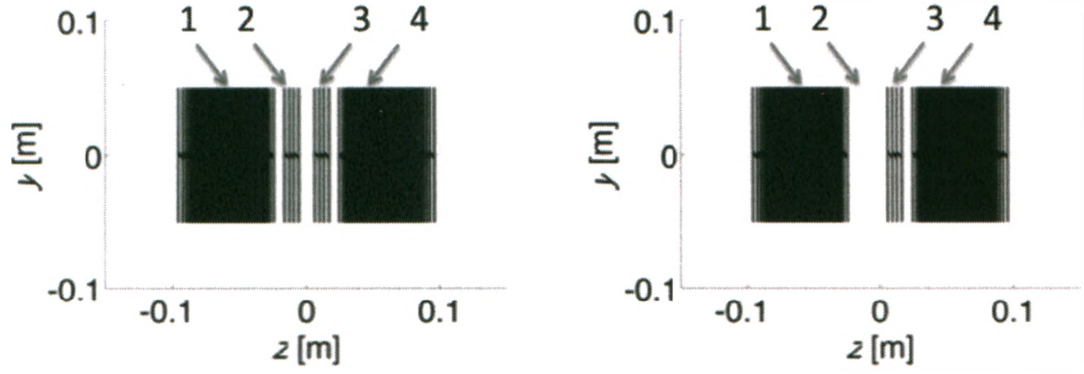

Figure 2.14: On the left is a fully functioning 5 cm radius Gz coil, on the right is the seventh operation mode that has had a short simulated in the 2nd quadrant, -0.02 < z < 0 for the 5 cm coil and -0.05< z < 0 for the 10 cm coil.

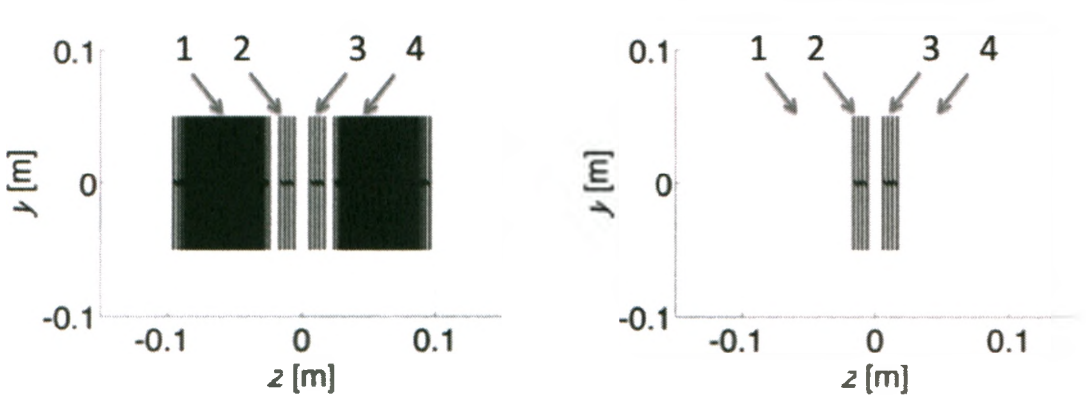

Figure 2.15: On the left is a fully functioning 5 cm radius Gz coil, on the right is the tenth operation mode that has had a short simulated in the 1st and 4th quadrant, z < -0.02 and 0.02 < z for the 5 cm coil and z < -0.05 and 0.05 < z for the 10 cm coil.

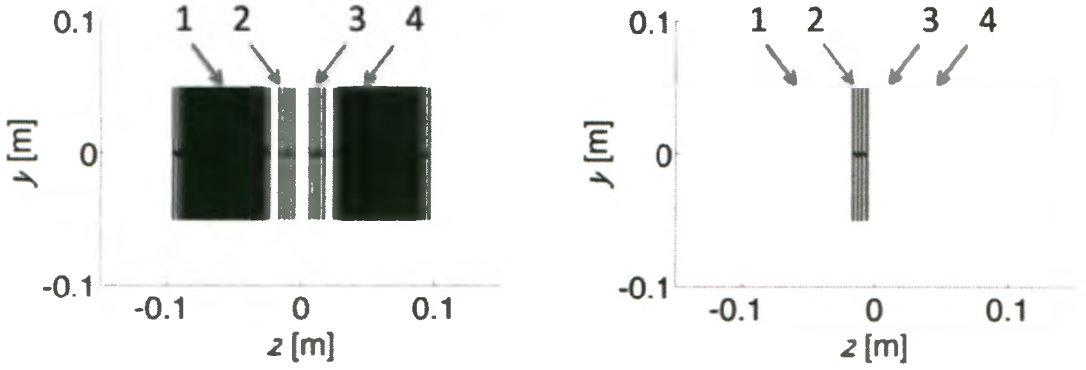

Figure 2.16: On the left is a fully functioning 5 cm radius Gz coil, on the right is the twelfth operation mode that has had a short simulated in the 1st, 3rd and 4th quadrant, z < -0.02 and 0 < z for the 5 cm coil and z < -0.05 and 0 < z for the 10 cm coil.

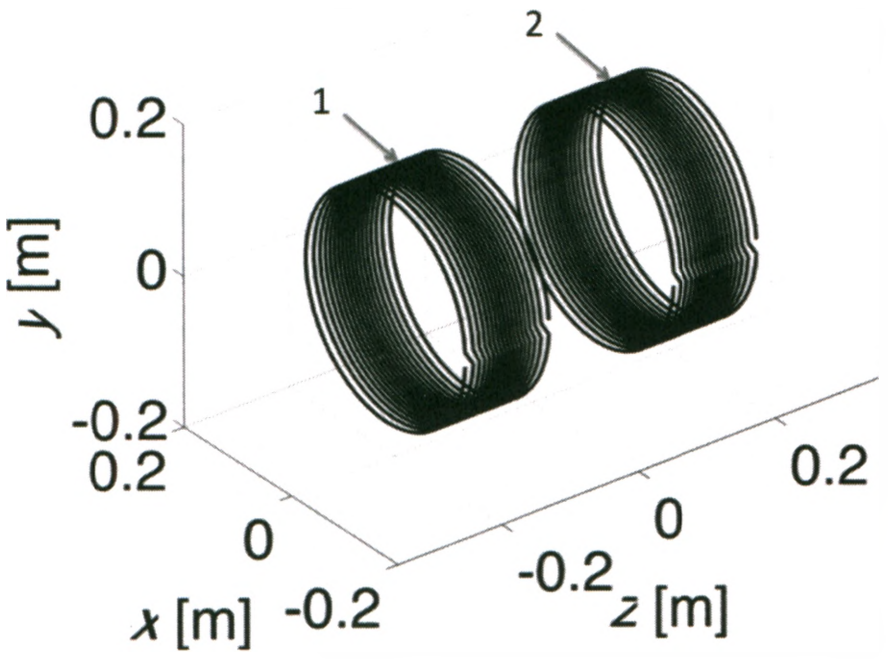

Figure 2.17: The fully functioning 15 cm radius Gz coil. The two current regions are indicated, and the 20 cm radius Gz coil showed the same trend in current distribution, but in different geometric locations.

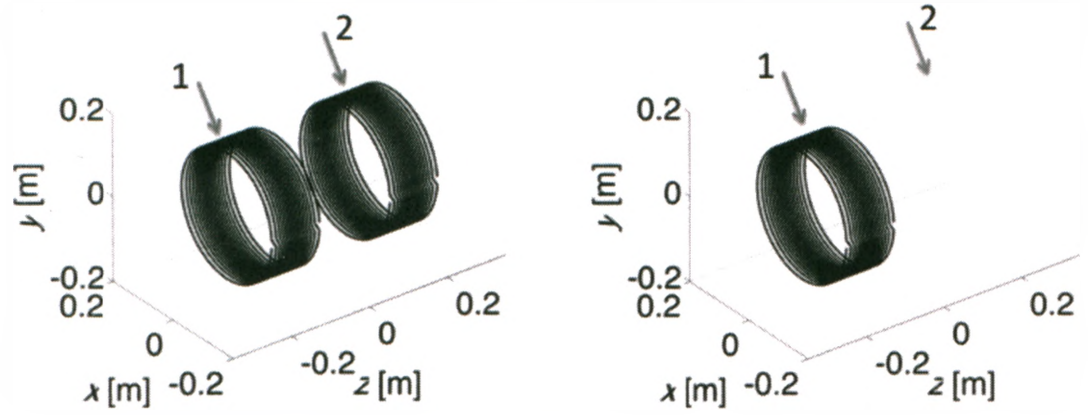

Figure 2.18: On the left is a fully functioning 15 cm radius Gz coil, on the right is the second operation mode that has had a short simulated in the 1st quadrant, 0 < z for the 15 cm coil and the 20 cm coil.

2.4.3 Implementing a Failure Mode:

With the physical locations of the failure modes established, the current in each wire segment in the desired quadrant was set to zero to simulate a short. Consider again the position matrix for the elements array, R. This matrix was divided into two groups, R_i for wire segments inside the failure region and R_o for the wire segments located outside the failure region. The current for each segment in R_i was then set to zero, and the new R_i' was combined with R_o to form the elements array for the failure mode, R_F.

2.5 Numerical Calculations:

2.5.1 Force and Torque Calculations Algorithm:

Equation [1.24] was used to calculate the net force on a gradient coil for a given location and orientation. The version of the Biot-Savart detailed by [1.19] was used for the necessary magnetic field calculations and [1.28] was used to calculate the torque on the insert coil. When calculating force and torque the following algorithm was used:

1) The above equations had their cross products evaluated using:

$$(a,b,c)\times(x,y,z)=\begin{vmatrix}\hat{i} & \hat{j} & \hat{k}\\ a & b & c\\ x & y & z\end{vmatrix} \qquad [2.4]$$

2) The insert coil was rotated about x by the desired amount, θ forming the rotated matrix R':

$$R'=\begin{bmatrix}\lambda\\ \lambda\\ 0\end{bmatrix}\times\begin{bmatrix}R\\ dR\\ I\end{bmatrix} \qquad [2.5]$$

3) The rotated elements array, R', was than translated to the preferred location forming R'':

$$R'' = R' + \begin{bmatrix} x_i \\ y_i \\ z_i \\ 0 \\ 0 \\ 0 \\ 0 \end{bmatrix} \qquad [2.6]$$

4) The magnetic field due to the main magnet was calculated using the first three rows of the R'' elements array, with the vector $\underline{r}$ being from the position elements of the main magnet to the position elements of the translated gradient insert.

5) The Lorentz force at each position element, rows 1-3 of R'', was evaluated by using rows 4 to 6 of the R'' elements array to dictate how the wire pattern is changing.

$$d\vec{F} = \begin{bmatrix} dFx_1 & dFx_2 & dFx_i & dFx_n \\ dFy_1 & dFy_2 & dFy_i & dFy_n \\ dFz_1 & dFz_2 & dFz_i & dFz_n \end{bmatrix} \qquad [2.7]$$

for: an insert with n wire segments.

6) The torque was then evaluated by using the force on each wire segment calculated in 5) and the first three rows of the R elements array for the position vector. For an even weighted coil, the origin (0, 0, 0) was taken to be the centre of mass of the insert coil.

7) Each row calculated in 5) was summed to find the components of force on the gradient coil, the net force on the coil was the sum of squares of each component of force

$$\vec{F} = \begin{bmatrix} Fx \\ Fy \\ Fz \end{bmatrix} = \begin{bmatrix} \sum (dFx_1 + dFx_2 + ... + dFx_n \\ \sum (dFy_1 + dFy_2 + ... + dFy_n \\ \sum (dFz_1 + dFz_2 + ... + dFz_n \end{bmatrix} \quad [2.8]$$

for: an insert with n wire segments. The net force on the insert coil was:

$$\left|\vec{F}\right| = \sqrt{Fx^2 + Fy^2 + Fz^2} \quad [2.9]$$

8) Steps 3-7 were repeated for every coil translation

9) Steps 2-8 were repeated for every insert coil rotation

10) Steps 2-9 were repeated for every coil operation mode

11) Steps 2-10 were repeated for every coil radius

12) Steps 2-11 were repeated for every coil type

2.6 Safe Region Calculations:

2.6.1 Safe Region-Force Threshold Determination:

It was determined that any force above 10 % the weight of the insert coil, may result in motion of the insert. The mass of the coil was estimated by assuming that average density of a potted coil was 2 g/cm^3, the density of a thermally conductive epoxy [4], and that potting increased the radius of the coil by 10 cm. It was assumed that the mass of the coil was predominately due to the epoxy layer, and the mass of the copper was insignificant. The volume of the potted coil was then used to find the total mass of the insert coils after fabrication. The effect of overestimating the mass of an insert coil will result in an overestimation in the size of the Safe Regions.

2.6.2 Safe Region - Torque Threshold Determination:

The Safe Region-Torque represented everywhere that the net torque on the gradient coil for every rotation and operation mode was less than the threshold. The mass of each coil was the same as for the force calculations above. The torque threshold was 10 % the force of gravity applied at a distance of 1 m to the centre of mass of the respective coil. The process of isolating the Safe Region-Torque and the Safe Region - Force were identical.

2.6.3 Safe Region Threshold Execution:

The calculated results were stored in a n_y x n_x x n_z array, where n_y, n_x and n_z were the number of divisions in the *y*-, *x*- and *z*- directions respectively. To threshold the data set, if the calculated net force was above the maximum allowable value then that result was set to zero in the array containing the force results. If the calculated value was below the threshold, then it was left as evaluated. This resulted in values that were zero, if they were above the threshold, and greater than zero for everything else in the force array. This process was done for every operation mode and every rotation and this process was repeated for the torque results.

2.6.4 Intersections of Data Sets to Determine a Safe Region:

The arrays containing the threshold force values were compared in sets of two. When both arrays had a force value above zero, this value was set to the threshold value, with any other force calculations set to zero. With both final arrays being identical, only one was needed to determine the overlap with the next data set. This process was repeated until every operation mode, for every rotation, had been compared between each other. By using a data array that contained either the threshold value or zero, the isosurface plot in Matlab was able to use zero as the critical value when determining the contours of the final Safe Regions. When the

overlap regions were determined, the final locations corresponding to the Safe Regions were isolated from the translation positions. This process was repeated for the torque calculations.

2.6.5 Combination of the Safe Region - Force and Safe Region - Torque:

The combination of Safe Region - Force and Safe Region Torque led to the final result of the Safe Region, where the net force, and net torque, on the insert coil for every rotation and operation mode were less than their respective thresholds. To do this the final array for Safe Region -Force and Safe Region - Torque were compared and any location where the arrays for both had a value above zero was kept as the threshold value, and any other data point was set to zero. The locations corresponding to these final threshold data points were used in the Safe Region plot, and zero was used as the critical value for the isosurface plots.

References:

[1]:Cheng, Yu-Chun N. et al (2004). A Comparison of Two Design Methods for MRI Magnets. *IEEE Transactions on Applied Superconductivity, 14*(3), 2008-2014

[2]: Chronik, Blaine A. et al (1998). Constrained Length Minimum Inductance Gradient Coil Design. *Magnetic Resonance in Medicine, 39*, 270-278.

[3]: De Bever, Joshua T. (2007). *Multiple-Imaging-Region Gradient Coil Insert for Parallel Imaging of Mice in MRI.* Unpublished masters dissertation, University of Western Ontario, Canada.

[4]:"Epoxies.com". 50-3100 High Thermal K Heat Transfer Epoxy Resin. http://www.epoxies.com/therm.htm (Aug 13/09)

[5]: Boas, Mary L. (1983). Toronto: *Mathematical Methods in the Physical Sciences 2nd Edition.* John Wiley & Sons

[6]: Young, Hugh D et al (2004). *University Physics 11th Edition.* Toronto: Pearson Addison Wesley

Chapter 3: Results

In this chapter the results will be displayed. These will range from the magnetic field profiles of the two main magnets to the Safe Region images. Through these figures and tables, the decision processes made to determine the Safe Regions should become a little clearer. The results for the main fields produced by the two main magnet designs, the transverse and longitudinal coils performance characteristics and positioning, the failure mode investigation, preliminary force and torque calculations on a 5 cm Gy coil operating normally and the Safe Regions will be displayed.

3.1 Magnet Representation:

To evaluate if the simplified main magnet was a suitable representation of the detailed magnet presented in sections 2.1.1 and 2.1.2 respectively, the magnetic field at different locations were calculated and compared for both designs. Figures 3.1 and 3.2 display the value of the magnetic field and the percent differences between the detailed and simplified magnets, for on- and off-axis locations respectively. The on-axis calculations were for points along the *z*-axis with no displacement along the *x*- or *y*-axis. The off-axis calculations were for points along the *z*-axis with displacements of 0.30 m along both the *x*- and *y*-axis. Figure 3.3 was the magnetic field maps for the simplified and detailed magnets through the *xy*-plane through the origin of the system.

a)

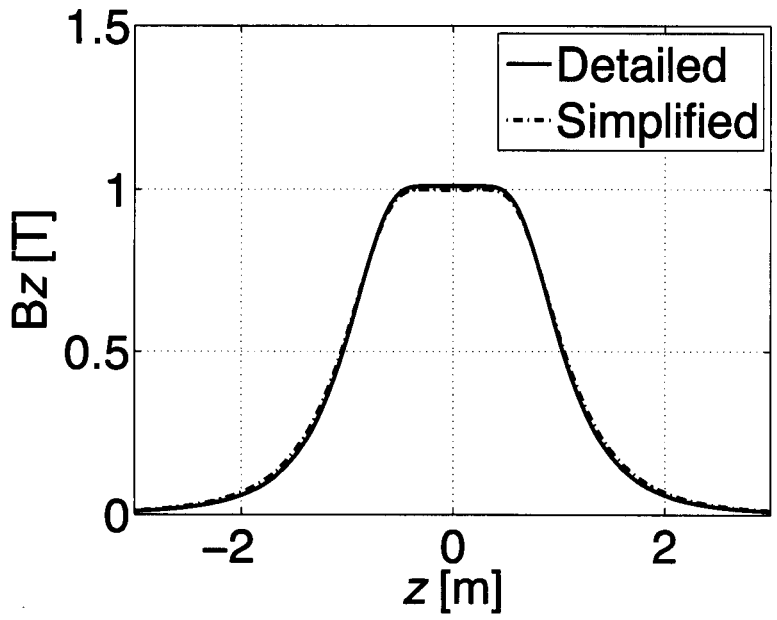

b)

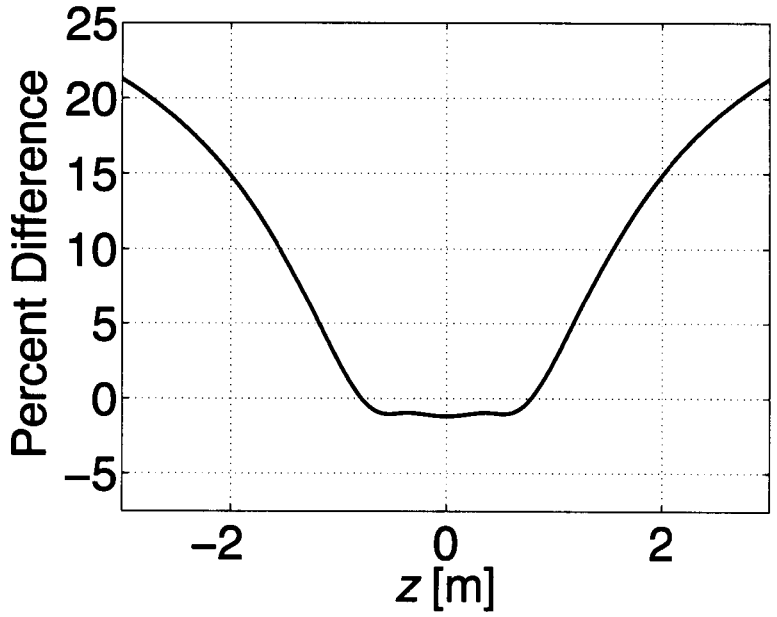

Figure 3.1 Magnetic Field Profiles; On-axis Calculations: a) the magnetic field profiles for the detailed and simplified 1-T main magnets. The Bx and By components of magnetic field were equal to zero. b) the percent difference in the simplified magnets Bz field compared to the detailed magnets Bz field, the peak difference of 21 % occurs at z = ± 3 m.

a)

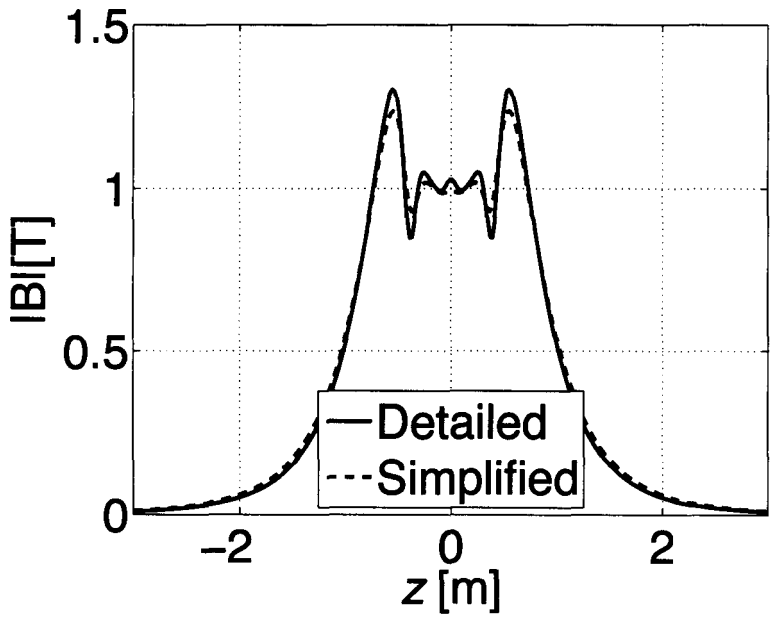

b)

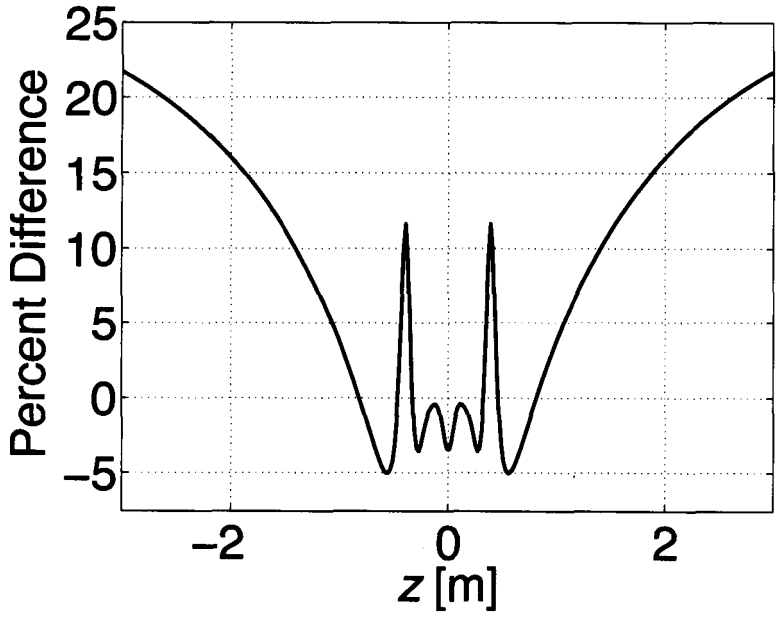

Figure 3.2 Magnetic Field Profiles; Off-axis Calculations: a) the magnitude of the magnetic fields produced by the detailed and simplified 1-T main magnets. The detailed and simplified representations have maxima of 1.30 T and 1.24 T at (0.3 m, 0.3 m, ±0.55 m) respectively. Both representations have Bx and By contributions present. b) the percent difference in the magnitude of the main field produce by simplified magnet compared to the detailed magnet. The peak differences of 22 % occur at (0.3 m, 0.3 m, ±3 m), and local maxima of 12 % occur at (0.3 m, 0.3 m, ±0.40 m).

a)

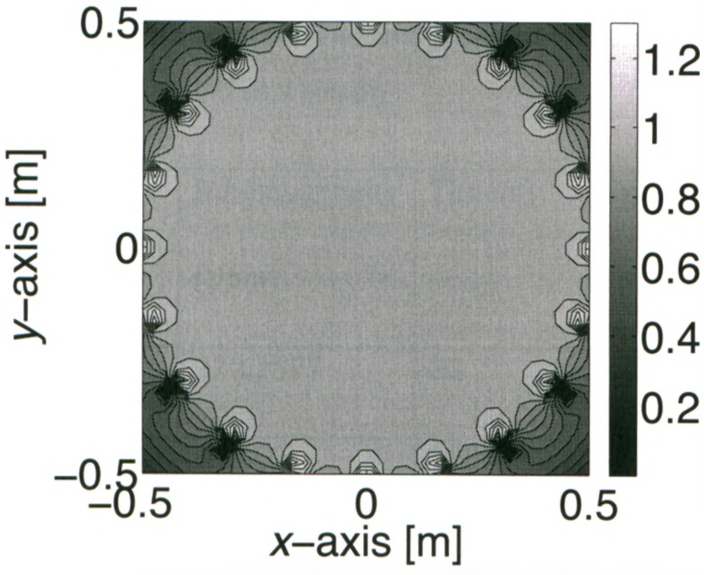

b)

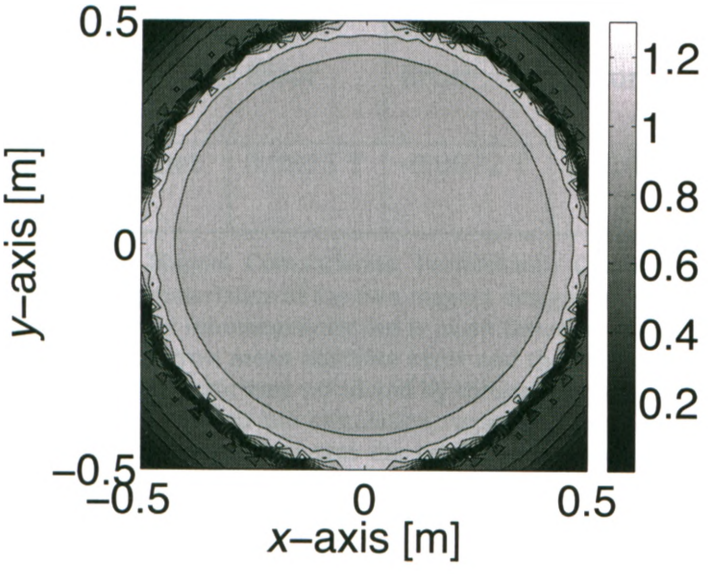

Figure 3.3 Magnetic Field Profiles; xy-plane Magnetic Field Map: The magnetic field map of the XY plane through (0, 0, 0) for the a) simplified main magnet and b) the detailed main magnet. Notice the smoother contours for the detailed main magnet, and how the wire segments can be seen for the simplified main magnet.

With speed of calculation becoming a factor when determining larger Safe Regions, the trade off between accuracy and speed becomes a factor. Table 3.1 displays the effects of a decreased inhomogeneity on the speed of calculations and the accuracy in the main field as a result.

a)

Magnet Representation	Inhomogeneity (ppm)	Time(s)	Speed Increase	Element Size
Simplified	272.2577	32	~3000	7x2280
Full Wire Represented Magnet	0.2652	91000	--------	7x5990151

b)

Magnet Representation	Max Error	Mean Error	Mean Absolute Error	Standard Error
Simplified Magnet	0.0815 T	-0.0072 T	0.0108 T	0.010 T

Table 3.1 Main Magnet Comparisons; Performance Characteristics: a) displays the performance characteristics of the two magnet designs presented. The down sampled magnet has a larger inhomogeneity but is much faster computationally. b) contains the max error, mean error, mean absolute error and the standard error in the simplified magnet design. The error was calculated by comparing paired magnetic field values for 20 000 random points in the calculation region for force and torque, as detailed in section 2.1.3. The times listed was the total time to calculate the field at all 20 000 points.

3.2 Gradient Coils:

The first of two types of coils investigated, figure 3.4, displays the wire patterns for the 4 different radii Gy coils considered. The performance characteristics are listed in table 3.2. The second type of coil investigated was the longitudinal coil, displayed in figure 3.5, with the performance characteristics listed in table 3.3. The total wire length was the amount of wire needed to build the desired coil, min wire separation was the smallest distance between two wires and the efficiency and inductance were discussed in section 1.3. The merit is a term used to compare coil design algorithms, the larger the merit the better the design algorithm.

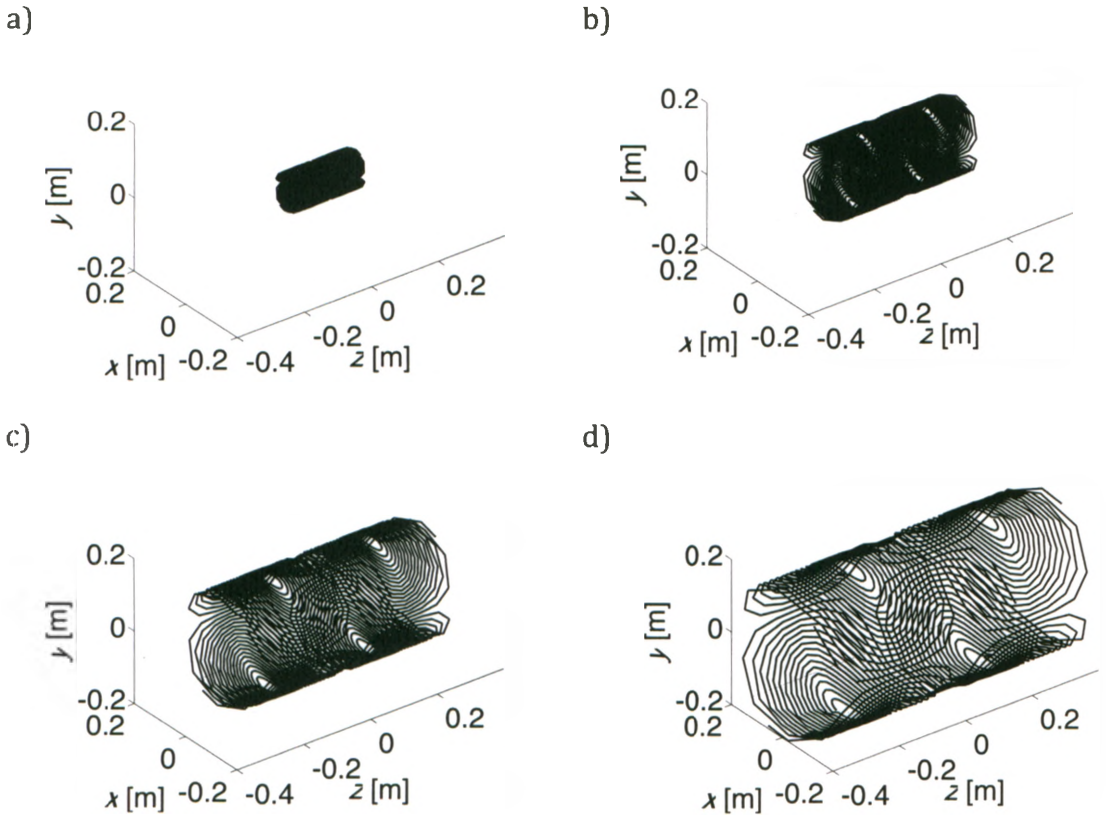

Figure 3.4 Transverse Coils, Gy: Clockwise from top left: 5 cm radius Gy coil, 10 cm radius Gy coil, 15 cm radius Gy coil and 20 cm radius Gz coil. All 4 coils had an AR=2.

Characteristic /Coil Radius (cm)	Total Wire Length (m)	Min Wire Separation (m)	Efficiency (mT/m/A)	Inductance (μH)	Merit ($mTm^{1.5}$/ H)
5	29	6.9e-04	8.3	214	0.317
10	41	0.0014	1.5	210	0.327
15	55	0.0021	0.59	240	0.334
20	61	0.0028	0.27	218	0.331

Table 3.2 Transverse Coils, Gy: Displays the characteristics of each Gy coil investigated in this study.

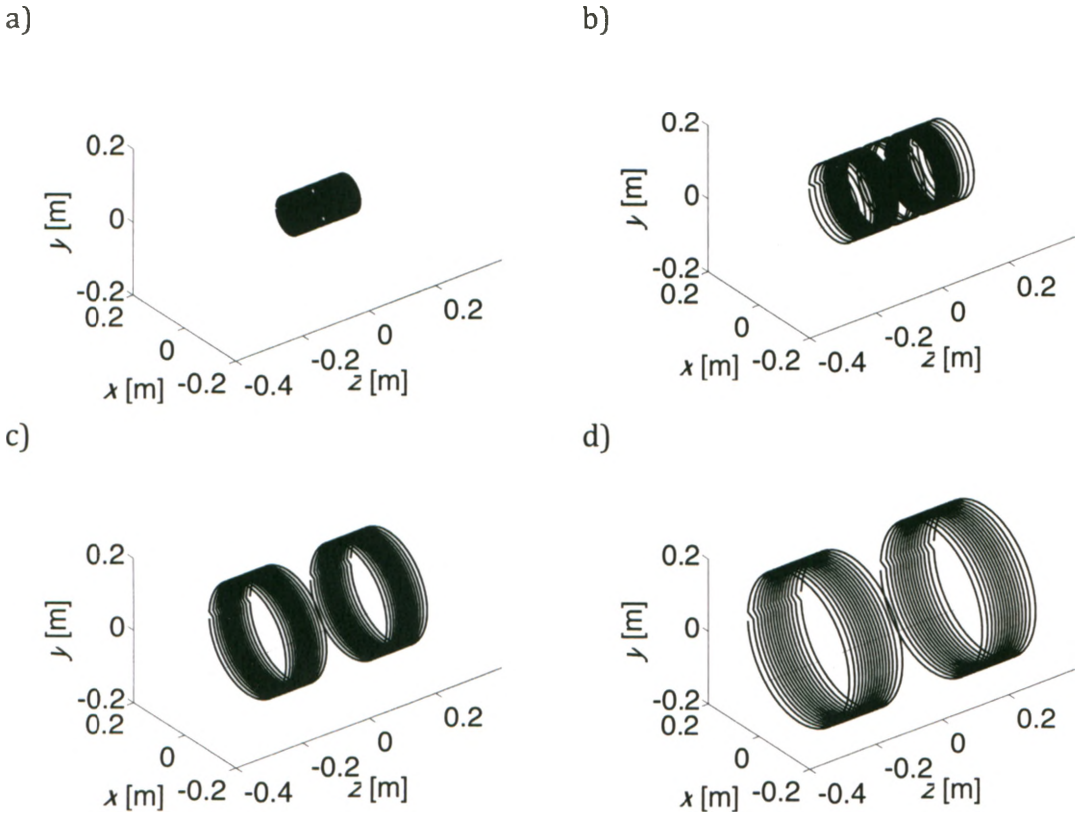

Figure 3.5 Longitudinal Coils, Gz: Clock-wise from top left: 5 cm radius Gz coil, 10 cm radius Gz coil, 15 cm radius Gz coil and 20 cm radius Gz coil. All coils had an approximate AR of 2.

Characteristic /Coil Radius (cm)	Total Wire Length (m)	Min Wire Separation (m)	Efficiency (mT/m/A)	Inductance (μH)	Merit ($mTm^{1.5}$/ H)
5	23	0.0010	7.9	191	0.319
10	34	0.0027	1.5	213	0.325
15	34	0.0056	0.53	196	0.326
20	40	0.0084	0.26	204	0.326

Table 3.3 Longitudinal Coils, Gz: Displays the characteristics of each Gz coil investigated in this study.

3.2.1 Gradient Coil Positioning:

With the physical parameters of the main magnet and the insert coils defined, the translation locations, and rotations were defined. When determining the maximum angle of rotation, the trade-off between the volume that the insert coil was going to be sampled in and the maximum misalignment was investigated. As the maximum angle of rotation increased, the volume of the translation region decreased. The maximum rotation of 23° was selected because it represented a large misalignment error while still allowing for a large enough centre of mass displacements. The parameters for the translation region were defined in figure 3.6. The finalized translation regions for each coil radii and type was summarized in table 3.4.

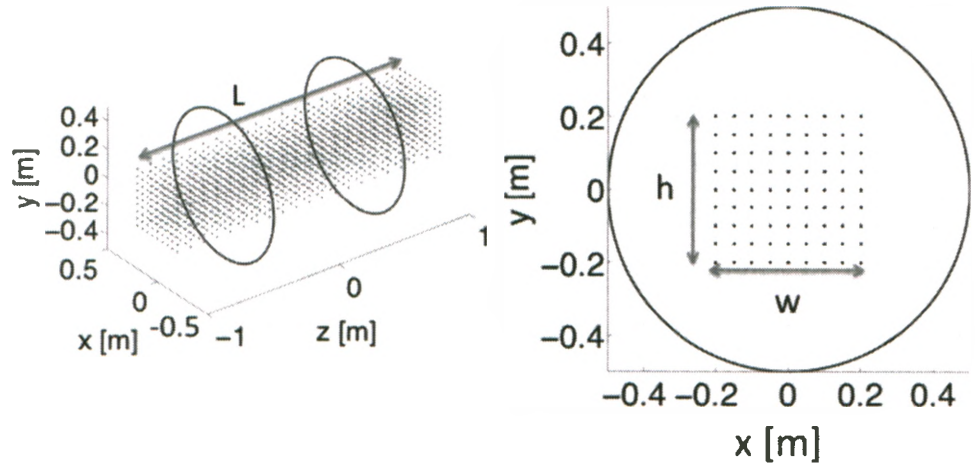

Figure 3.6: On the left the length of the translation is shown for a 5cm radii coil. The translation region represents all the locations that the gradient coils centre of mass was translated to when determining the Safe Regions. The image on the right is the XY projection of the translated region, and shows the height and width of the region. For every coil radius the translation region had a square projection, so h=w.

Parameter/ Coil Radius, AR	r_e (m)	largest x, y (m)	chosen x, y (m)	closest approach (m)
5 cm , AR = 2	0.085	0.29	0.20	0.13
10 cm , AR = 2	0.17	0.23	0.15	0.12
15 cm , AR = 2	0.255	0.17	0.10	0.10
20 cm , AR = 2	0.34	0.11	0.05	0.09

Table 3.4: Displays the final parameters of the chosen translation regions for the 4 basic coil geometries investigated. The effective radius was for the maximum chosen rotation of 23° about the *x*-axis. The largest *x*- and *y*- axis displacements possible for a rotation of 23° about the *x*-axis are shown above, as well as the maximum displacements chosen for those axis. *x*- and *y*- axis. The closest approach represents the closest that the insert coil came to the main magnet at the maximum displacement point, for the largest rotation investigated.

3.3 Failure Modes:

The assumption was made that a full short in the failure region of a coil would result in the largest forces and torques on an insert coil. In order to validate this assumption, the force and torque on an insert coil was calculated as the current in the failure region was increased from 0 A, full short, to 1 A, normal operation. The current in rest of the insert coil was maintained at 1 A. The centre of mass of each insert coil investigated was translated to (0, 0 , 0.5 m). For each set of figures, the force on the insert coil is on the right, and the torque on the left. For the Gz coils investigated, the magnitude of torque was on the order of magnitude of Matlabs floating point precision.

The net force on the Gy coils were all at a minimum for a short and linearly increased to the maximum for normal operation. The peak torque on the Gy coils varied based on operation mode. The operation modes were then separated into expected and unexpected results.

The Gy operation modes were plotted in figures 2.3-2.7. The 5 cm radius Gz coil operation modes were plotted in figures 2.8-2.16 and the operation modes for the 15 cm radius coil was plotted in figure 2.17 and 2.18.

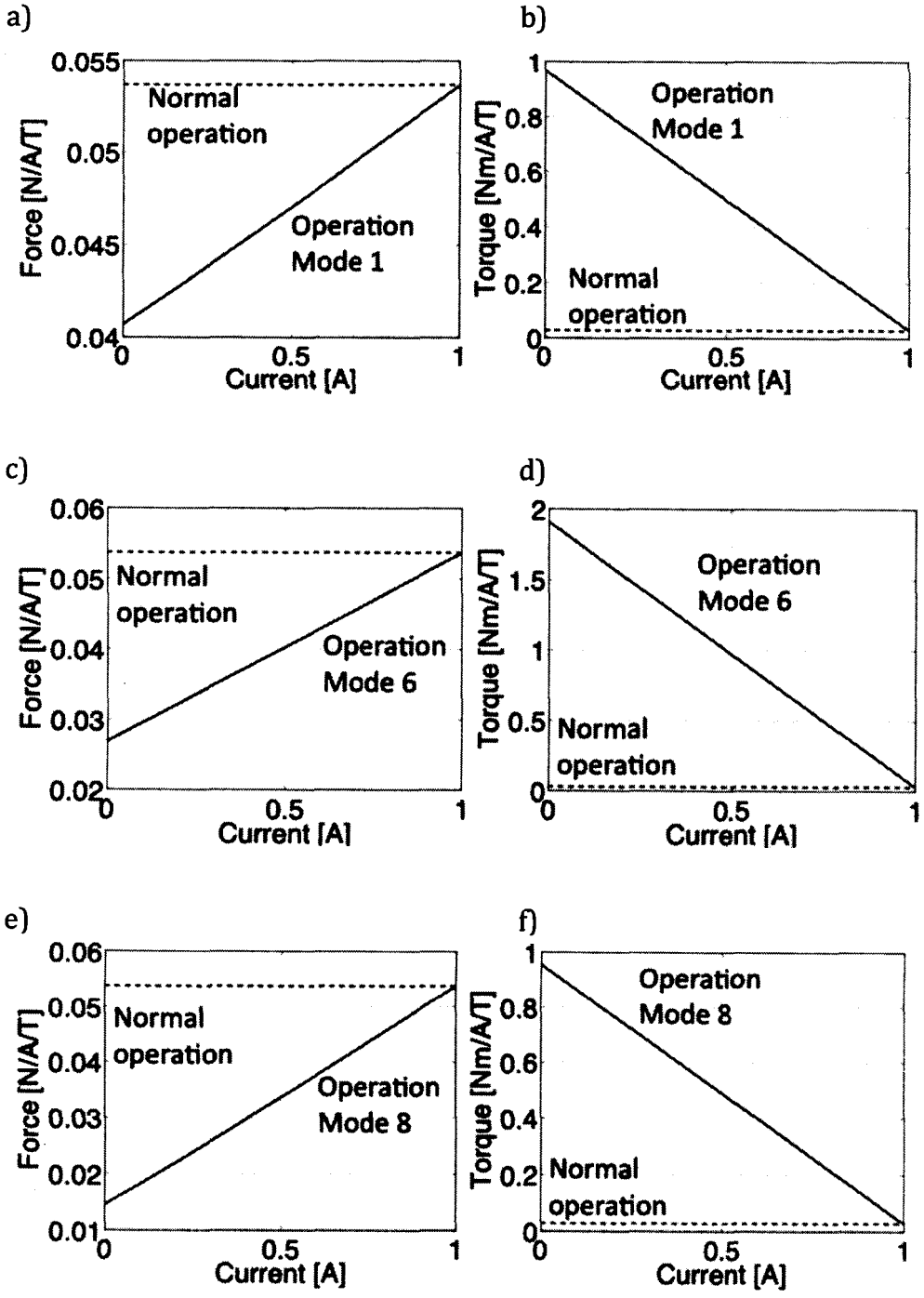

Figure 3.7 Gy Failure Mode Investigation; Expected Results: While the force on the insert coil during each operation mode was still an unexpected result, the torque on the insert coil followed the expected result of being maximum for the full short and then decreasing to normal operation values as the current is increased in the failure region.

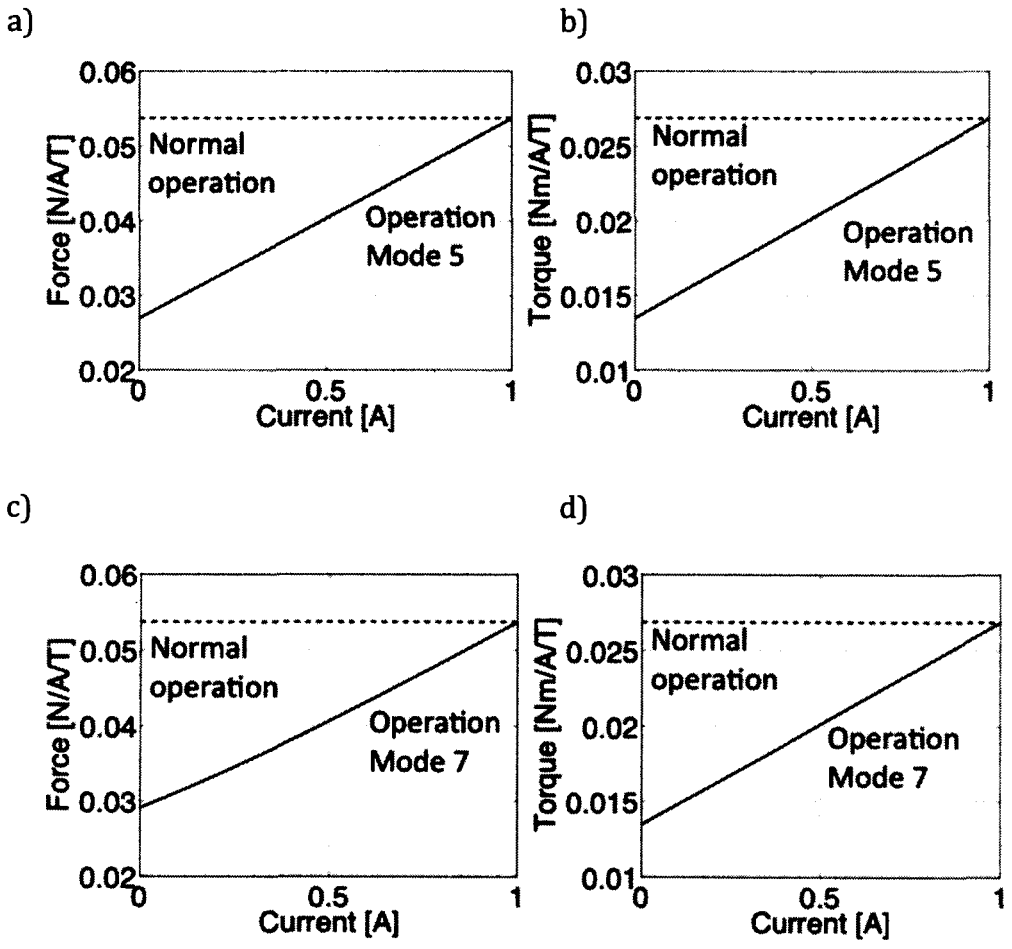

Figure 3.8 Gy Failure Mode Investigation; Unexpected Results: The two operation modes for the Gy coil that displayed the unexpected result of a minimum torque for the full short, and a maximum for normal operation. The force still displayed the expected result.

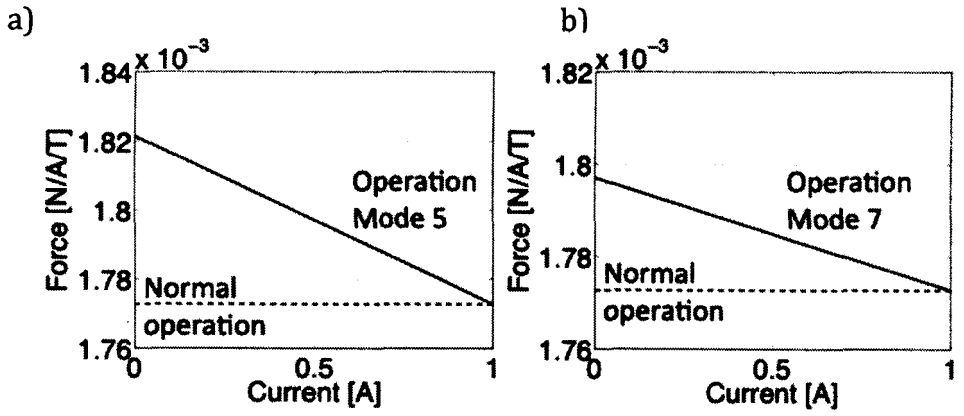

Figure 3.9 Gz Failure Mode Investigation; Expected Results: Operation mode 5 and 7 showed the expected result of a maximum force on the insert coil for a full short.

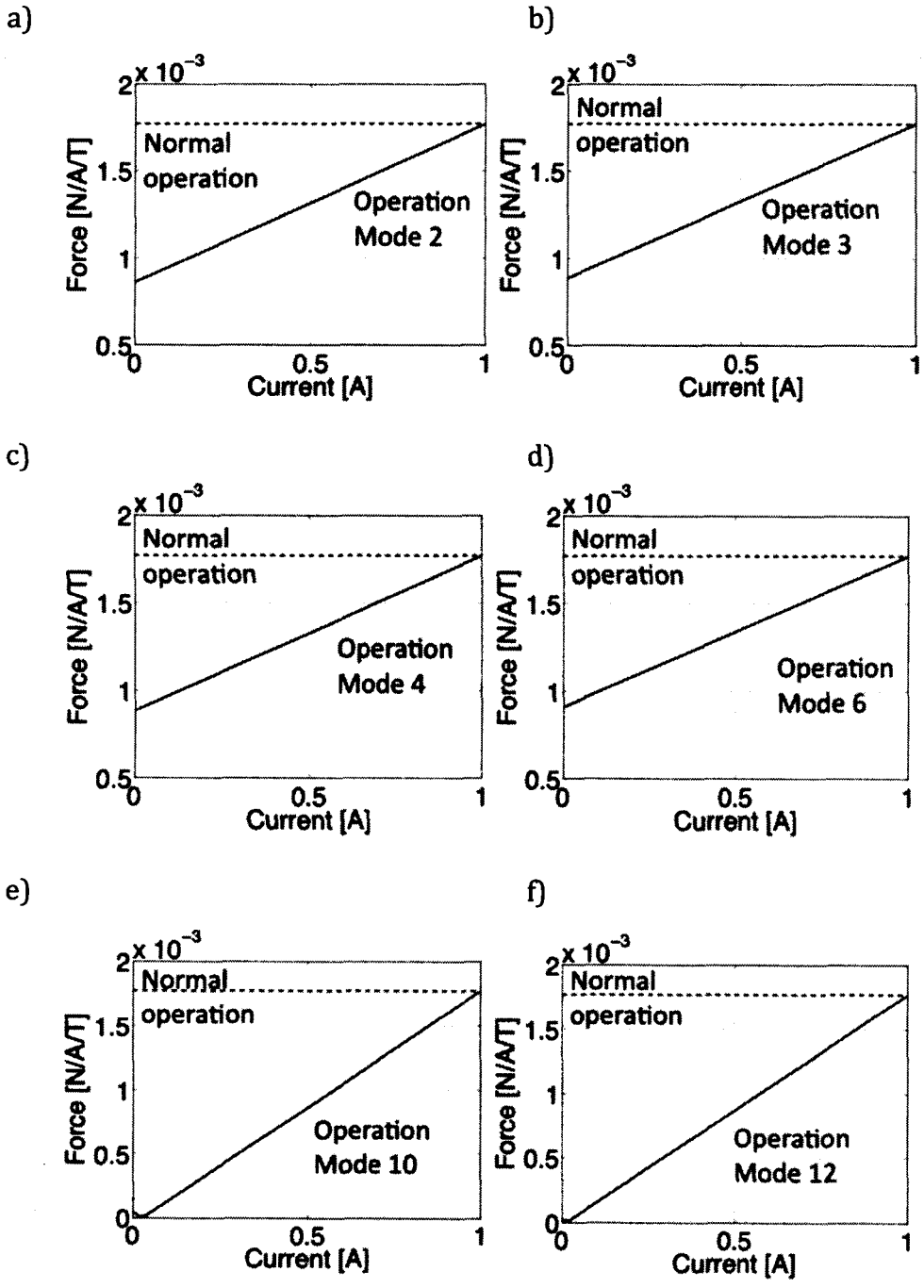

Figure 3.10 Gz Failure Mode Investigation; Unexpected Results: Operation mode 10 and 12 differed from the other unexpected results by both having a decreasing force on the insert coil, before it increased to the maximum value for normal operation.

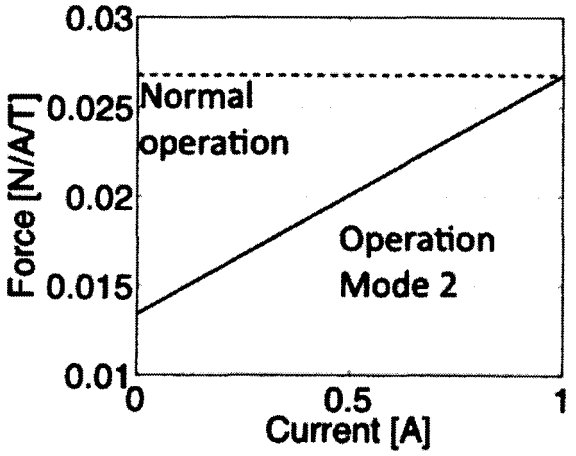

3.11 Gz Failure Mode Investigation; 15 cm radius Gz coil: The 15 cm Gz coil showed a maximum force on the insert coil for normal operation

3.4 Preliminary Force and Torque Calculations:

Through the following sets of figures, the force and torque on an insert coil were shown for different positions, and orientations in the main magnet. The insert coil was a 5 cm radius Gy coil with an inductance of 214 μH and an AR of 2 that was operating normally. For the on-axis calculations the insert coils centre of mass was translated to different positions along the *z*-axis, and the force and torque was evaluated at each of these positions. The off-axis calculations involved an initial translation of the insert coil, and then the positions were varied along the *z*-axis in the same way as the on-axis calculations.

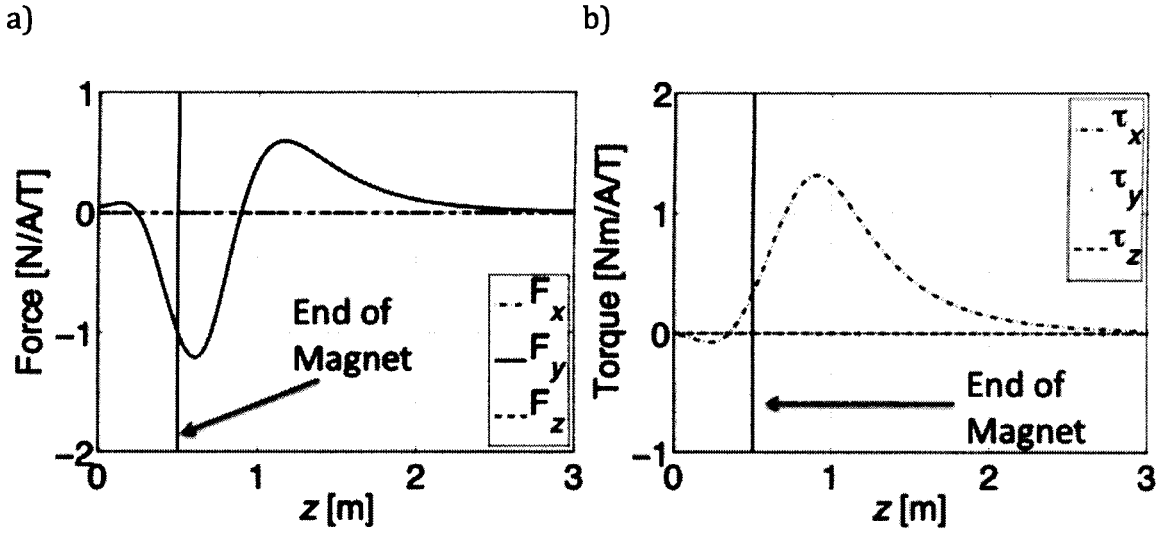

Figure 3.12 Force and Torque; On-axis with no rotation: The peak force on the coil was F_y= 1.2 N/A/T at (0, 0, 0.61 m) and the peak torque was τ_x = 1.3 Nm/A/T at (0, 0, 0.91 m).

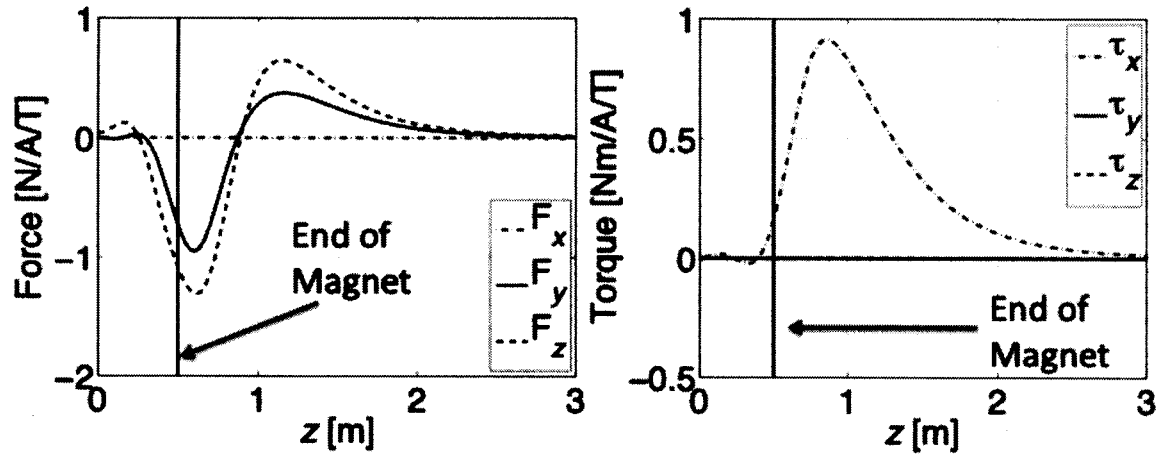

Figure 3.13 Force and Torque; On-axis with a rotation of 23° about the x-axis: The peak componet's of force on the coil were F_y= 0.95 N/A/T at (0, 0, 0.61 m) and F_z= 1.3 N/A/T at (0, 0, 0.61 m) and the peak torque was τ_x = 0.91 Nm/AT at (0, 0, 0.85 m).

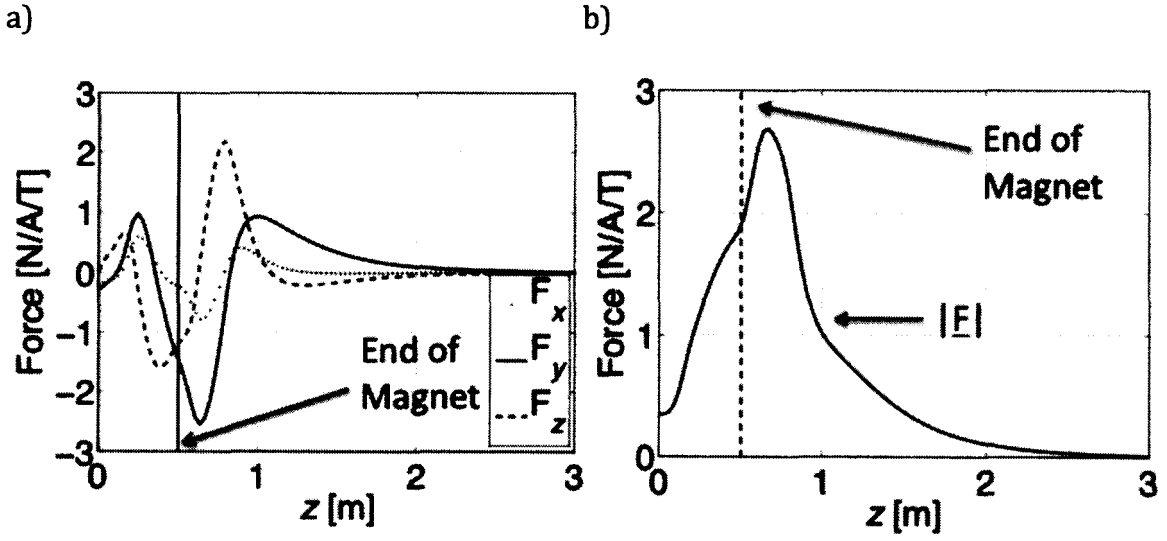

Figure 3.14 Force; Off-axis displacement of (0.2 m, 0.2 m, 0 m) with no rotation: The peak magnitude of force on the coil was 2.7 N/A/T at (0.2 m, 0.2 m, 0.67 m).

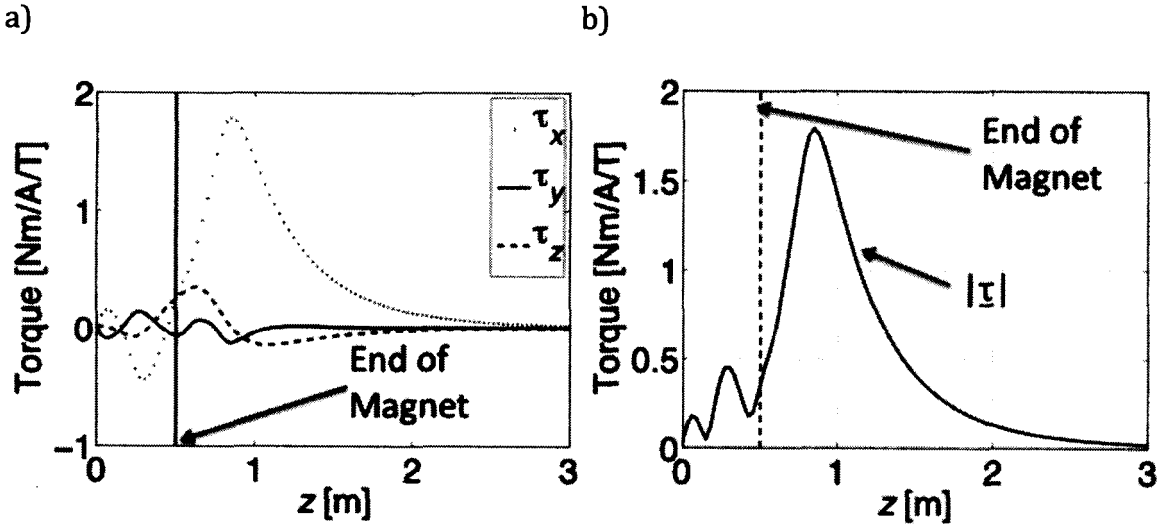

Figure 3.15 Torque; Off-axis displacement of (0.2 m, 0.2 m, 0 m) with no rotation: The peak magnitude of torque on the coil was 1.8 Nm/A/T at (0.2 m, 0.2 m, 0.85 m).

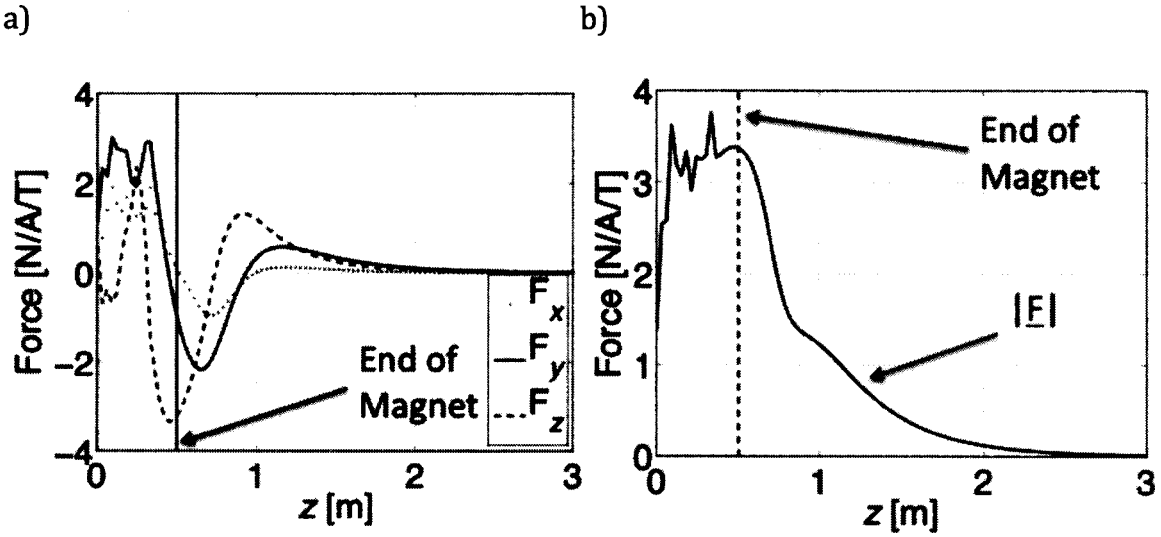

Figure 3.16 Force; Off-axis displacement of (0.2 m, 0.2 m, 0 m) with a rotation of 23° about the *x*-axis: The peak magnitude of force on the coil was 3.8 N/A/T at (0.2m, 0.2m, 0.33 m).

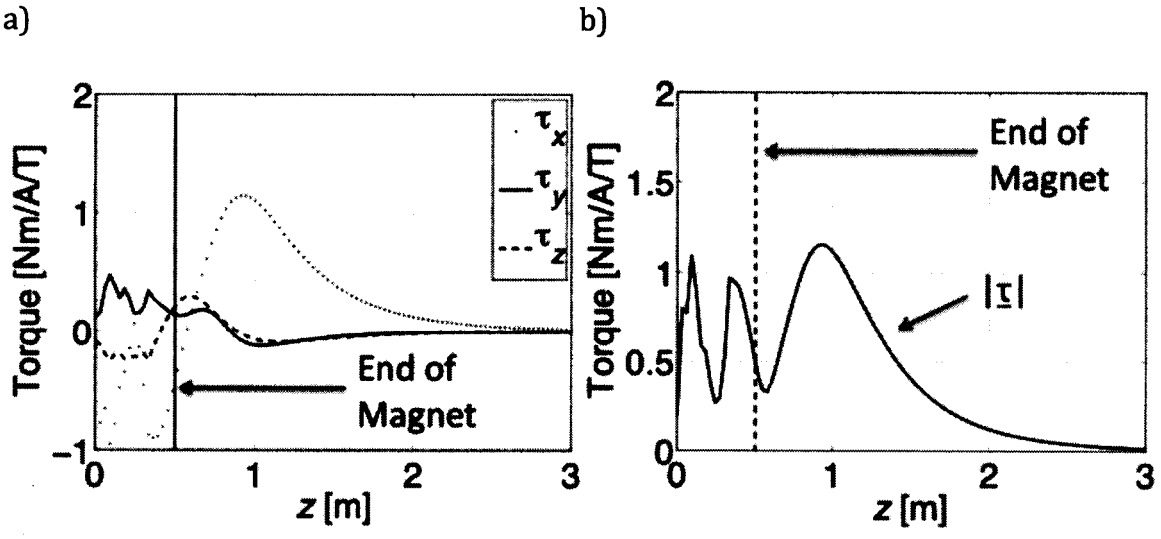

Figure 3.17 Torque; Off-axis displacement of (0.2 m, 0.2 m, 0 m) with a rotation of 23° about the *x*-axis: The peak magnitude of torque on the coil was 1.2 Nm/A/T at (0.2 m, 0.2 m, 0.94 m).

3.5 Safe Regions:

The last set of figures are the Safe Region plots. The mass of the 5 cm, 10 cm, 15 cm and 20 cm radius coils were 12.5 kg, 25 kg, 50 kg and 100 kg respectively. The force threshold was 10 % the force of gravity and the torque threshold was 10 % the force of gravity applied at a distance of 1 m to the centre of mass for each insert coil investigated. With a typical insert coil carrying 300 A of current during usage in typical field strengths of 3.0 T, the results were scaled to better fit the expected implementation of these small animal insert coils.

The Safe Region-Force for every insert coil, except the 20 cm radius Gy coil, had 2 distinct regions outside the cold bore limits, while the Safe Region-Torque extended further outside the isocentre of the main magnet. The intersection of the Safe Region-Force and the Safe Region-Torque was clearly seen in every Safe Region.

In figure 3.26 an expanded region was shown for the 5 cm Gy insert coil that has had the *z* range increased to [-5 m, 5 m] while maintaining the other translation, rotation parameters and the thresholds. Notice that at larger distances from the main magnet, the Safe Region - Force and Safe Region - Torque has expanded. Intuitively this should make sense, as the magnetic field has decayed to a few percent of the main field value.

a)

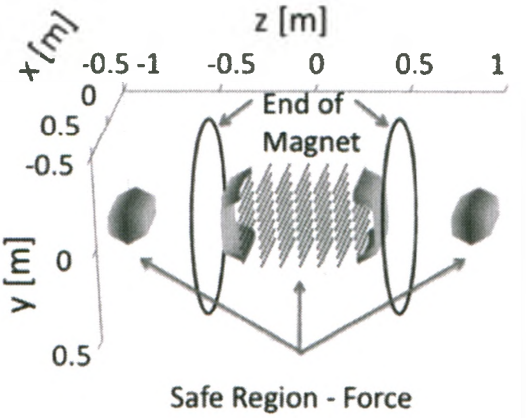

Safe Region - Force

b)

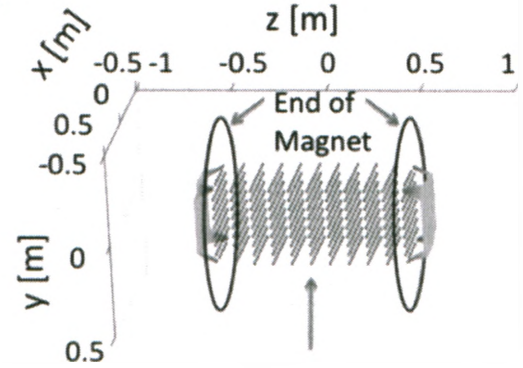

Safe Region – Torque

c)

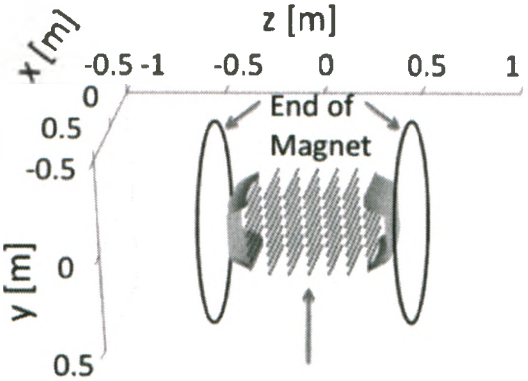

Safe Region

Figure 3.18 Safe Region; Transverse Insert Coils; 5 cm radius coil: Top to bottom: Safe Region-Force, Safe Region-Torque and the Safe Region for the 5 cm radius Gy coil.

a)

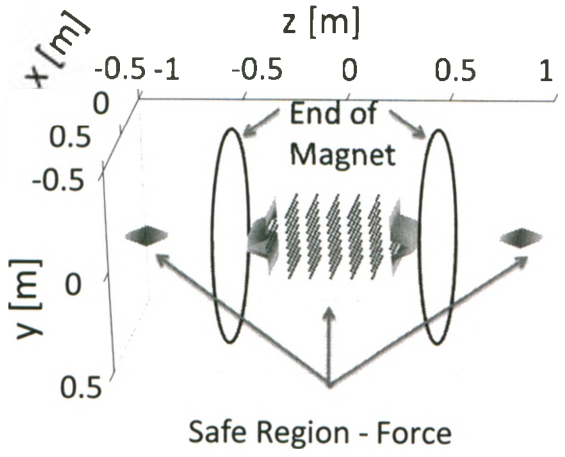

b)

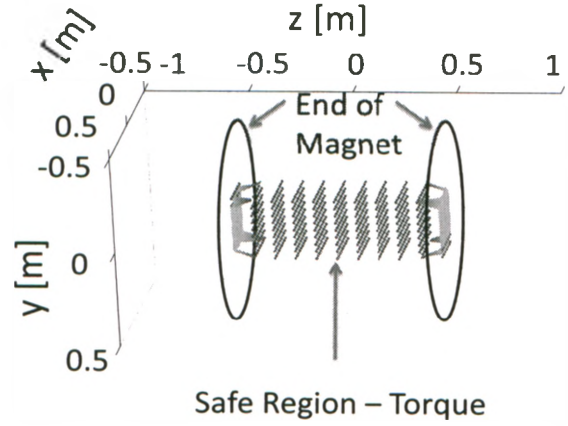

c)

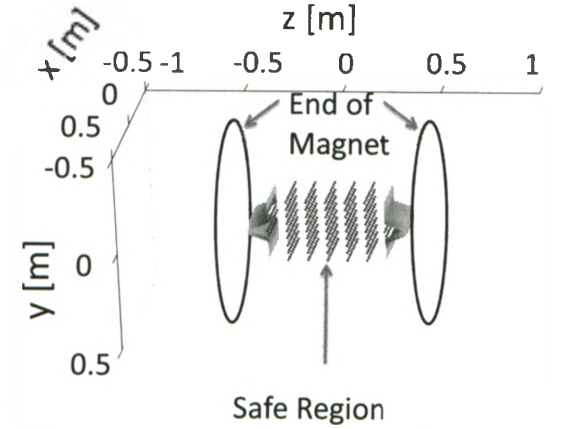

Figure 3.19 Safe Region; Transverse Insert Coils; 10 cm radius coil: Top to Bottom: Safe Region-Force, Safe Region-Torque and the Safe Region for the 10 cm radius Gy coil.

a)

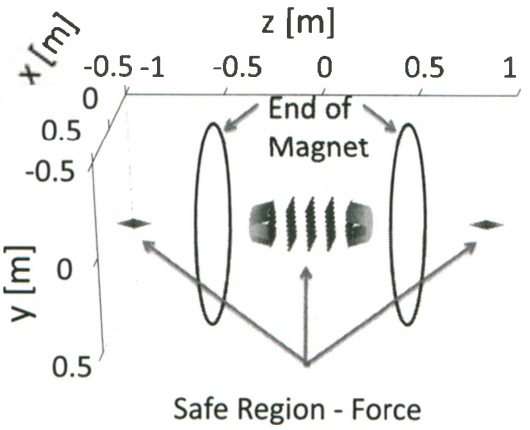

Safe Region - Force

b)

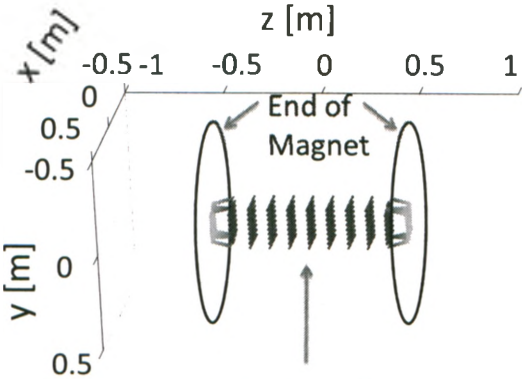

Safe Region – Torque

c)

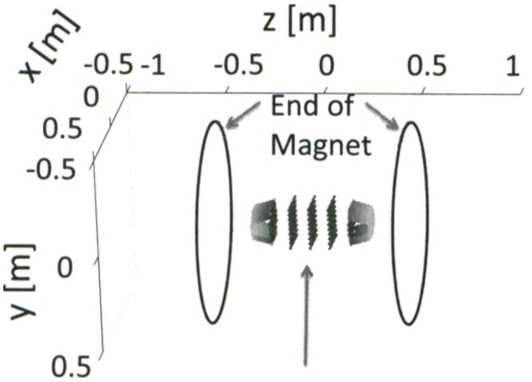

Safe Region

Figure 3.20 Safe Region; Transverse Insert Coils; 15 cm radius coil: Top to bottom: Safe Region-Force, Safe Region-Torque and the Safe Region for the 15 cm radius Gy coil.

a)

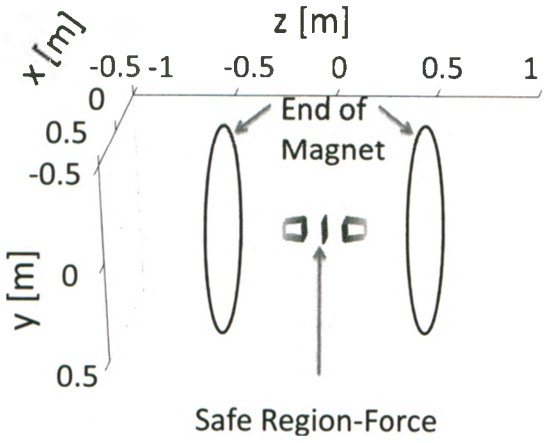

b)

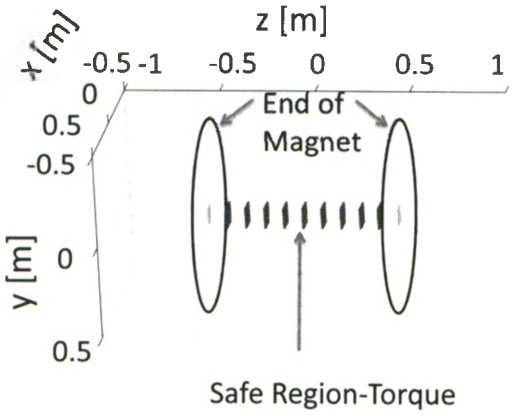

c)

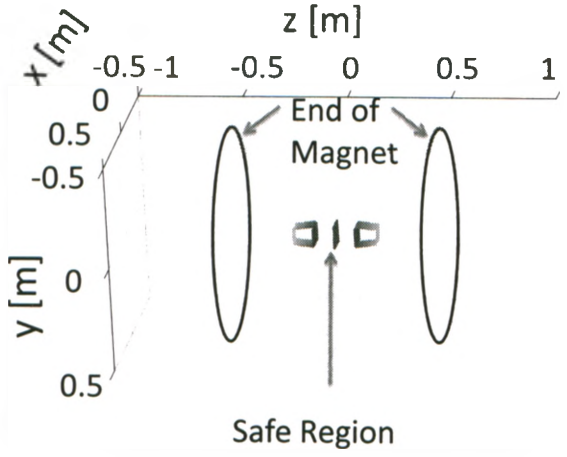

Figure 3.21 Safe Region; Transverse Insert Coils; 20 cm radius coil: Top to bottom: Safe Region-Force, Safe Region-Torque and the Safe Region for the 20 cm radius Gy coil.

a)

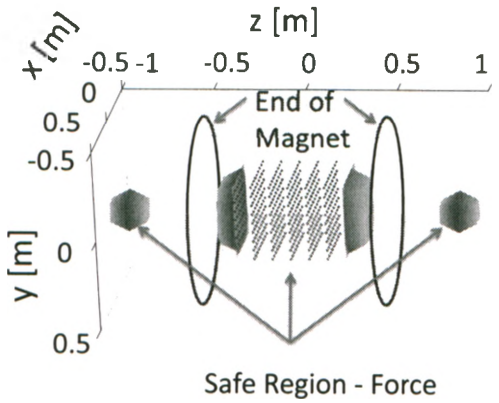

b)

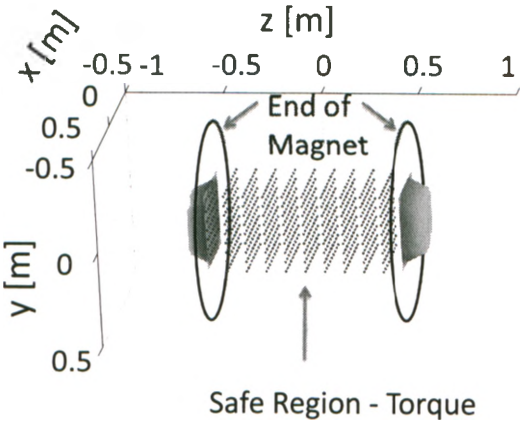

c)

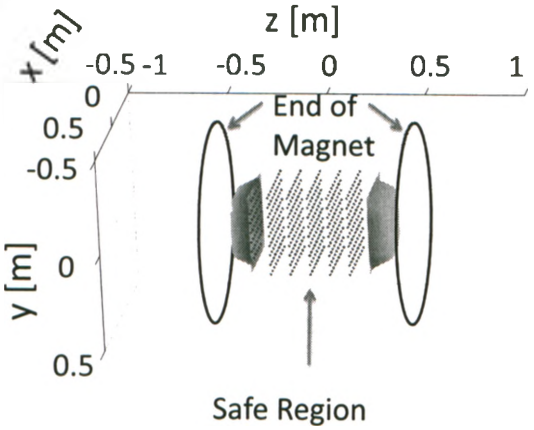

Figure 3.22 Safe Region; Longitudinal Insert Coils; 5 cm radius coil: Top to Bottom: Safe Region-Force, Safe Region-Torque and the Safe Region for the 5 cm radius Gz coil.

a)

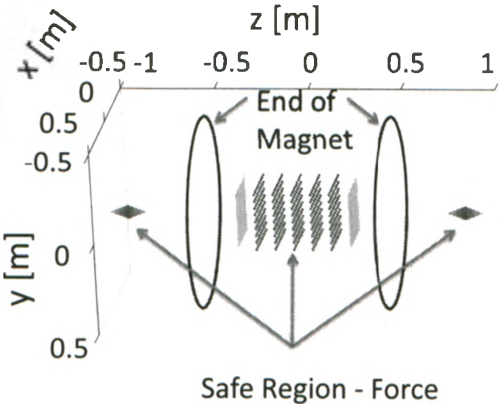

Safe Region - Force

b)

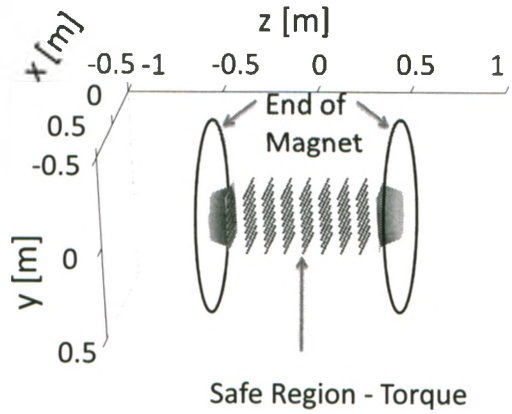

Safe Region - Torque

c)

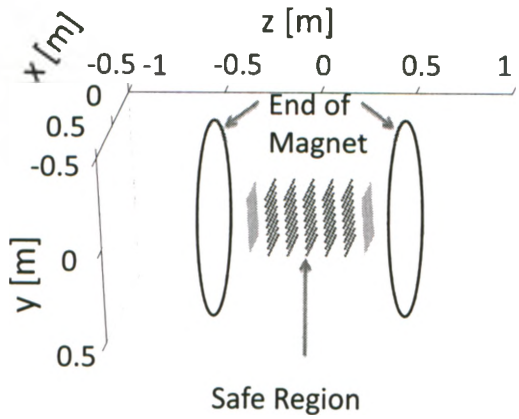

Safe Region

Figure 3.23 Safe Region; Longitudinal Insert Coils; 10 cm radius coil: Top to bottom: Safe Region-Force, Safe Region-Torque and the Safe Region for the 10 cm radius Gz coil.

a)

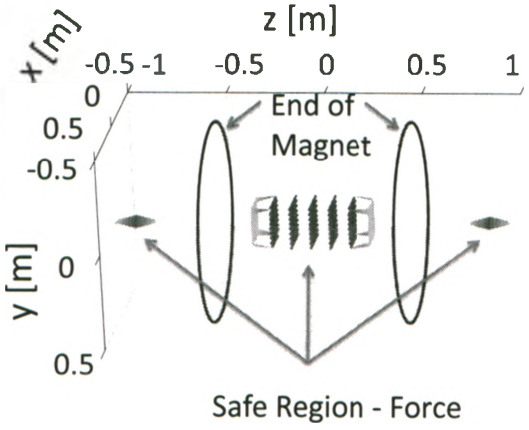

Safe Region - Force

b)

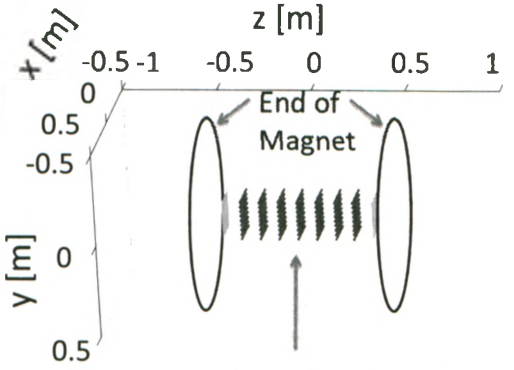

Safe Region - Torque

c)

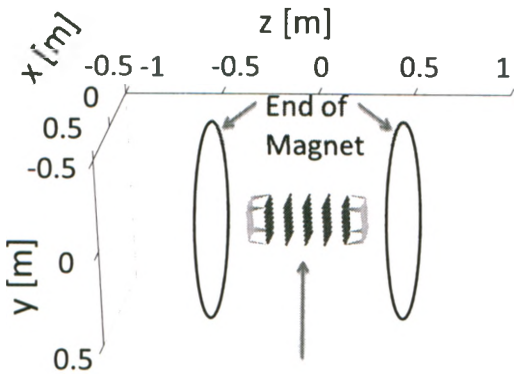

Safe Region

Figure 3.24 Safe Region; Longitudinal Insert Coils; 15 cm radius coil: Top to bottom: Safe Region-Force, Safe Region-Torque and the Safe Region for the 15 cm radius Gz coil.

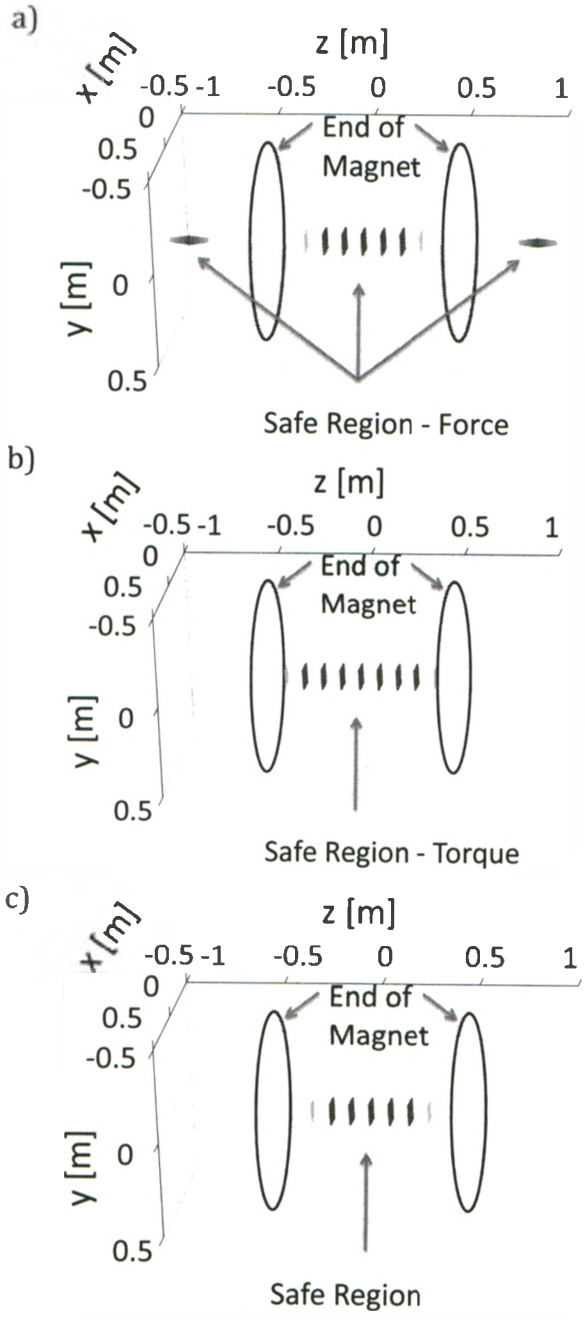

Figure 3.25 Safe Region; Longitudinal Insert Coils; 20 cm radius coil: Top to bottom: Safe Region-Force, Safe Region-Torque and the Safe Region for the 20 cm radius Gz coil.

a)

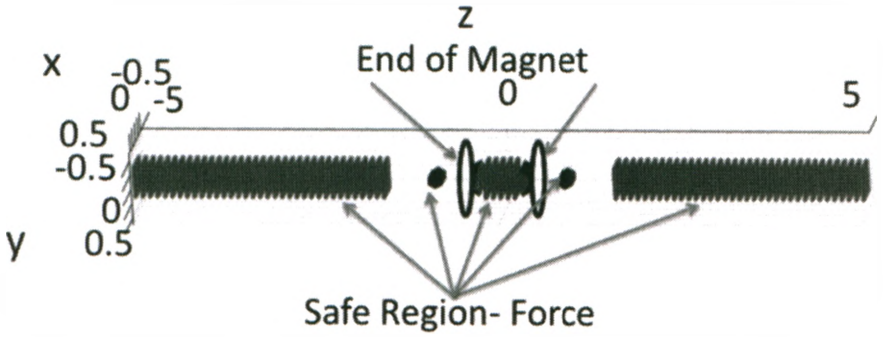

b)

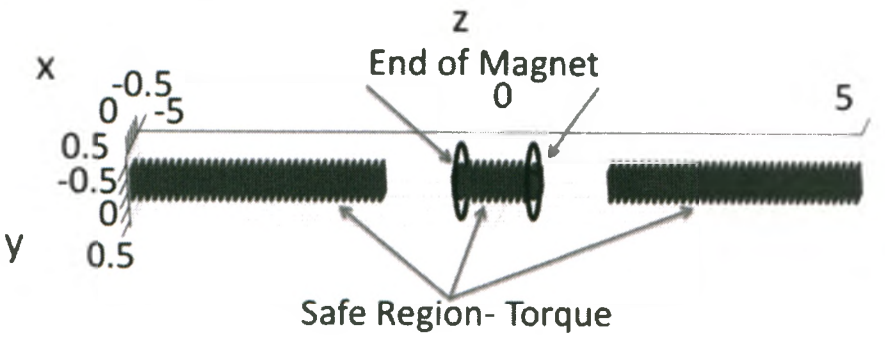

c)

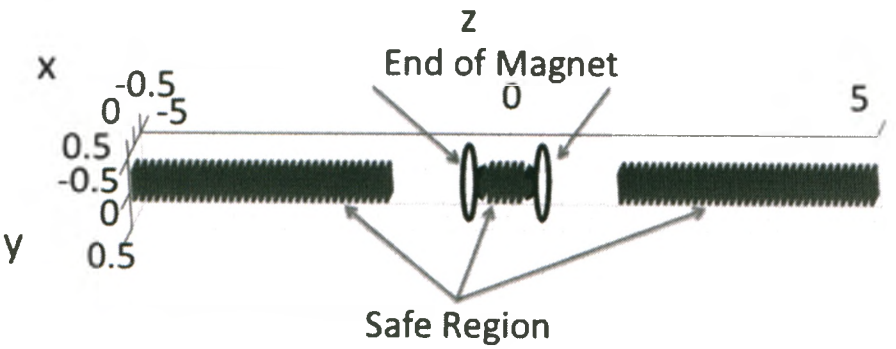

3.26 Expanded Safe Region; 5 cm Radius Gy Coil: The Safe Region-Force, Safe Region-Torque and the Safe Region for the 5 cm radius Gy coil with an expanded translation region. For positions where the insert coils centre of mass has been translated to $z > 1.6$ m or $z < -1.6$ m the net force and torque on the insert coil are less than their respective thresholds.

3.6 Safe Region; Summary:

For each insert coil considered, the isocentre of the main magnet was completely enclosed in the Safe Regions. There was also a large region surrounding the Safe Regions, which indicates the flexibility in positioning of an insert coil. In table 3.5 the parameters of the Safe Regions are displayed. Along the *x*- and *y*- axis the Safe Region's dimensions extend to the furthest displacement considered, see table 2.3, and so mis-placements along the *x*- and *y*- axis are not a determining factor of insert safety. This is encouraging because it allows for a large flexibility in insert coil positioning.

From the expanding Safe Region results, the danger in insert coil operation is when it is initially being moved into the bore. From about 1.5 m from the magnet isocentre, to where the magnet begins is the region that insert coil operation can be considered dangerous. These results were only calculated for the 5 cm radius Gy coil, but should hold true for every coil type. In this region the field has the largest degree of variation, and so the largest forces and torques should occur in this area.

Coil Type: Radius (cm)	$x_{\text{Safe Region}}$ (m)	$y_{\text{Safe Region}}$ (m)	$z_{\text{Safe Region}}$ (m)
Gy: 5	[-0.20, 0.20]	[-0.20, 0.20]	[-0.30, 0.30]
Gy: 10	[-0.15, 0.15]	[-0.15, 0.15]	[-0.30, 0.30]
Gy: 15	[-0.10, 0.10]	[-0.10, 0.10]	[-0.20, 0.20]
Gy: 20	[-0.05, 0.05]	[-0.05, 0.05]	[-0.10, 0.10]
Gz: 5	[-0.20, 0.20]	[-0.20, 0.20]	[-0.30, 0.30]
Gz: 10	[-0.15, 0.15]	[-0.15, 0.15]	[-0.20, 0.20]
Gz: 15	[-0.10, 0.10]	[-0.10, 0.10]	[-0.20, 0.20]
Gz: 20	[-0.05, 0.05]	[-0.05, 0.05]	[-0.20, 0.20]

Table 3.5 Safe Region Size Parameters: Displays the sizes of the Safe Regions for all 8 insert coils considered. The $x_{\text{Safe Region}}$, $y_{\text{Safe Region}}$ and $z_{\text{Safe Region}}$ are the ranges of centre of mass locations that describe the final Safe Region for each insert coil, they are for the *x*-, *y*- and *z*-axis respectively.

References:

[1]:Cheng, Yu-Chun N. et al (2004). A Comparison of Two Design Methods for MRI Magnets. *IEEE Transactions on Applied Superconductivity, 14*(3), 2008-2014

[2]: De Bever, Joshua T. (2007). *Multiple-Imaging-Region Gradient Coil Insert for Parallel Imaging of Mice in MRI.* Unpublished masters dissertation, University of Western Ontario, Canada.

[3]: Chronik, Blaine A. et al (1998). Constrained Length Minimum Inductance Gradient Coil Design. *Magnetic Resonance in Medicine, 39*, 270-278.

[4]: Young, Hugh D et al (2004). *University Physics 11th Edition.* Toronto: Pearson Addison Wesley

Chapter 4: Discussion

In this chapter, we summarize the results from Chapter 3, and make recommendations for regions within which gradient coil operation is most safe.

4.1 Main Magnet Representation:

All of the results presented in this thesis depend on the accuracy with which the main magnet is represented. It is important that the magnet design used be relevant to the clinical systems most commonly used with gradient inserts. A defining feature of the main magnets used in MRI systems is the high degree of field uniformity they possess. This fact prohibited us from using typical simple representations, such as the Helmholtz pair or a sufficiently long solenoid. The field profiles produced by these much simpler electromagnets would have resulted in

force and torque results irrelevant to the evaluation of the safety of gradient inserts in real MRI systems.

Typically, the actual designs of commercial MRI magnets are not publically available; furthermore, there is not a large body of academic literature in which realistic whole-body MRI magnet systems are investigated. The main magnet design presented by Cheng et al. [1] provided a good initial start to finding a way to represent the main field. The magnet presented had physical dimensions that were judged close enough to a realistic design that it was considered acceptable for this purpose.

Another approach would have been to physically measure the magnetic field produced by a commercial system to which we have access, and use that data set for the force and torque calculations. This would involve experimentally determining the field at different locations through the bore, and then using an interpolation scheme to find any field values for locations that were not directly measured. This approach would certainly have been valid and would be a consideration for future work in this area. For the purposes of this thesis, this approach was considered too time-consuming and was not pursued.

A practical difficulty with using the exact design detailed in [1] was the speed of magnetic field calculations. Using the model presented in [1], it took approximately 91 000 seconds to compute 20 000 magnetic field values using a standard desktop computer. For the analysis of a typical insert gradient coil, 2000 magnetic field values were calculated for each centre of mass location. For each operation mode the force was calculated at 1701 different centre of mass locations, and this was done for all 5 coil rotations and every operation mode. For a Gy coil this corresponds to 51 030 total force calculations for a given coil radius, for a total time of 460 000 000 seconds or 128 000 hours or 5300 days. The preliminary speed estimations made it clear that a simpler magnet representation would be necessary for this project.

In producing the simplified magnet model, the overall geometry of the magnet needed to be preserved while decreasing the number of current windings. In addition, the relative current in each of the 10 component solenoids that comprise the main magnet needed to remain fixed. By decreasing the number of current elements in the magnet model, the number of steps in the Biot-Savart Law decreases linearly, resulting in shorter computation times for all field calculations. The challenge was to assure that the fields produced by the simplified model were sufficiently accurate, particularly in off-axis locations.

When deciding how to down-sample the main magnet, the field produced by a single current carrying solenoid was used to compare fields produced by the full representation versus the down-sampled versions. We found that by using groups of circular loops in place of a solenoid, with one set placed at the inner radius and another placed at the outer radius and a third added at the middle radius, that calculation speed was increased while only introducing a small amount of error in the field. The separation along the z-axis for each circular loop was set to be at most 5 % of the inner radius of the respective solenoid. The average difference calculated over a set of 20 000 random points was found to be only 10 mT and yielded a speed increase of about 3000. The largest percent difference in the two fields calculated was 22%, and this occurred at the points (0.3 m, 0.3 m, ±3 m). The speed increase of approximately 3000 times allowed for a complete data set for a given gradient coil to be calculated in approximately 150 000 s or 1.8 days.

The difference in fields obtained using the simplified magnet model as compared to the detailed model from [1] is very likely less than differences between magnets from different commercial vendors. This needs to be verified in a more comprehensive analysis. In addition, it should be clear that the results of this study are entirely based on a traditional, actively-shielded, cylindrical whole-body MRI system. Systems that are smaller (such as head-only MRI systems), or unshielded, would be expected to lead to different results. Most dramatically, systems of very

different geometry such as the "open" MRI systems where the field orientation is vertical, would be entirely different.

4.2 Gradient Coil Representations:

The Gy coils were all obtained using a simple Stream Function Method [2]. An advantage of this method allows the direct control of a wire pattern of the coil, and in particular its length. The designs obtained using this method are realistic and fully representative of standard gradient coil inserts. There was no need to separately design and analyze Gx coils, as they are a simple rotation of the Gy coils.

The Gz coils were obtained using a Fourier Series method with constrained length [3]. This method constrains the maximum length a coil may have; however, it does allow for shorter coils. The result of this was an inability to exactly specify the AR of the Gz coils. In all cases, the final lengths of the Gz coils were close to having an AR of 2.

As discussed in Chapter 2, the number of windings used on each coil was adjusted such that the final coil had an inductance as close to 200 μH as possible. The inductance of a coil is proportional to the number of wire contours squared, and the problem was that only integer wire contours are allowable. This meant that the final inductance could not generally be scaled exactly to 200 μH. By having insert coils with similar inductances, they can be considered to have the same stored energy, which allows for a more equal comparison of final force and torque results across coil radii. The specific inductance value of 200 μH was chosen because this is the lower-end of typical inductances used for insert gradient coils. By choosing a value on the lower-end of the typical range allowed for a reduction in the number of elements necessary to represent the gradient coils, and thereby reduced the calculation time.

All of the gradient designs used in this study were not actively shielded. The presence of an active shield would have had a significant impact on this study. First of all, it would have introduced a much larger number of possible failure modes. Secondly, the forces and torques calculated for any given modes would be very different than for the unshielded case. In practice, all whole-body gradients used in MRI are actively shielded; however, for gradient inserts, there is much more variation. In the insert gradients developed and used in the laboratories at the University of Western Ontario, it is typical not to include active shielding in the designs [4]. Because one of the primary motivations of this work was to evaluate the safety of these insert gradient coil applications, it was determined that unshielded coil designs should be focused on. Inclusion of active shielding would represent an opportunity to extend this project in the future.

4.3 Gradient Positioning:

The degree that an insert coil could be rotated within the bore of a scanner depended on the radial displacement of the coil. In order to compare Safe Regions across coil types and radii, each coil was to undergo the same rotations. The limiting case for the maximum angle of rotation was the 20 cm radius Gy coil with an aspect ratio of 2 because it was the largest coil and had the lowest flexibility in rotations and mis-positions. An angle of 23° was chosen as the maximum angle of rotation. It was felt that this was a large enough rotation to represent a catastrophic mis-positioning error while still yielding enough flexibility that enough positioning errors could still be investigated.

The maximum calculated x and y displacements for the 20 cm Gy coil were 0.10 m for a total width of 0.20 m. The chosen values are much smaller than this at 0.05 m max displacements and a total width of 0.10 m. This was done because the numerical results of the Biot-Savart magnetic field calculations become inaccurate if evaluated too close to the wire segments. In order to compensate for this all of the

coil translations were selected to be at least 5 cm further away from the cold bore limit.

4.4 Failure Modes:

4.4.1 Implementing failure modes

In the context of this study, a failure mode was defined as a change in the current density as compared to a normally operating coil. The final goal was to find under what conditions the Lorentz force and resultant torque on an insert coil was small enough that operation of the coil can be considered safe. When considering failure modes, only changes to the coil that will change the Lorentz forces and torques on the coil were considered important.

When determining how the current distribution could change during a failure mode, plots of the insert coils were used to evaluate the positions of the return wires. For a Gy coil an electrical short can occur when a return wire makes contact with an earlier part of the coil. This short will change the current distribution because current will no longer flow through one or more quadrants. This allows each quadrant of the coil to be a possible source of failure. If only full shorts and normal current flow are assumed in the quadrants of interest then a 4 fingerprint Gy coil will have 16 operation modes. With only the magnitude of force and torque of interest in determining the Safe Regions the number of operation modes was reduced from 16 to 6. By only being concerned with the magnitudes of force and torque, a short in one fingerprint quadrant should result in the same net force and torque on the insert coil regardless of what quadrant shorts. This results in the five failure modes; one quadrant short, one horizontal half shorts, one vertical half shorts, diagonal quadrants short and shorts in three quadrants.

The failure modes for Gz coils were determined in the same manner as Gy coils, by planning out return wires that may cause a short. In order to decrease the

computation time, symmetry was used to decrease the number of Gz operation modes. For the 5 cm and 10 cm Gz coils, there were additional distinct current-carrying regions. This corresponded to a larger number of operation modes for these coil radii and type compared to the same radii Gy coils. Considering only the magnitudes of force and torque, the same assumption was made for the Gz coils that were made for the Gy coils when determining failure modes.

The assumption was that a full short (i.e. 0 A of current) in a failed region would result in the largest net forces and torques on the insert coil because this would most result in a highly unbalanced coil. In an effort to validate this assumption the coil was translated to the extreme limits of the cold bore, a position that was known to result in unbalanced forces and torques. At this location the relative current in a failed quadrant was increased incrementally from 0 A to 1 A. The force and torque on the insert was calculated for each current input, this was repeated for every operation mode in the coil. The results were shown in figures 3.7-3.11. The transverse coil considered was the 5 cm radius coil. All 4 different Gy coils had essentially identical current distributions, so when testing the symmetry of the transverse coils, one Gy coil would be sufficient. With the Gz coils having two different current distributions, one with each distribution was chosen to test the different failure modes.

4.4.2 Failure Mode Investigation: Gy coils:

The net force on the Gy axes was found to always be a maximum for normal operation. The net force increased linearly from the value for the shorted coil, to the maximum value for normal operation. This result was unexpected, as the assumption was that the forces for a fully symmetric coil operation would generally sum to near zero. The reason for the observed effect is that within a relatively uniform magnetic field, each individual quadrant of the gradient coil is approximately force-balanced. When a coil is moved into a region of more non-

uniform magnetic field, there are unbalanced forces on each individual quadrant. In this later case, by reducing one or more of the quadrant currents to zero, the net force actually decreases. In general, this result suggests that for transverse coils it is actually the coil positioning that is more important when considering net forces on the structure, as opposed to specific failure modes.

When considering the net torque on the Gy coils, it should be noted that even in a completely uniform magnetic field, each individual quadrant of the coil is highly unbalanced. When individual quadrants are combined, the total torque may increase or decrease depending on the relative current directions within those quadrants. For the combination of two quadrants on the same end of the coil (i.e. both with $z > 0$, or both with $z < 0$), the torque on the two normally operating quadrants will add. For the combination of two quadrants on the same "side" of the coil (i.e. both on the top or the bottom of the coil), the torque on the two normally operating quadrants will cancel. This behavior was observed in the Results of the previous chapter.

4.4.3 Conclusion: was a short the worst case?

While there were mixed results as to whether or not a short was the worst possible operation mode, an important observation was made: peak forces and torques were occurred for either full shorts or normal open ration modes only. When evaluating the safety of an insert coil under failure conditions, this allows us to simplify the analysis and only investigate "full shorts" and "normal operation", ignoring all partial short cases.

4.5 Force and Torque for Longitudinal Displacements Only:

The initial results were a simple plot of the force on an insert at varying locations of centre of mass along the *z*-axis. These calculations were relatively quick, while giving insight into the geometry of the problem and how it relates to spatial positions relative to the main magnet. It is also important to consider simply longitudinal displacements as they are the most common type of misalignment expected during everyday use of insert gradient coils.

4.5.1 General Direction of Forces and Torques

For the transverse (Gy) gradient coils aligned with the magnet the only net component of force was F_y. The component of current responsible for producing the changing *z*-component of magnetic field in the Gy gradient coils is always the azimuthal component. For our main magnet design, with each solenoid aligned with the *z*-axis, the field produced was cylindrically symmetric. This explains why the net $F_x = F_z = 0$ for every coil position investigated for on-axis calculations with no rotation.

It was expected that the peak force should be when the coil was in the most unbalanced field, and that this should be near the limits of the physical bore. The field on the outer limits of the magnet will have decreased significantly as compared to the fields closer to the center of the magnet. This was situation in figure 3.12a, as the peak force occurred when the insert coil centre of mass was located at (0 m, 0 m, 0.61 m).

The torque on the Gy coils had one major contributing component, τ_x. The winding pattern comprising a Gy coil is essentially a series of approximately circular loops oriented in the *x*-*z* plane. If these loops are thought of as magnetic moments, the magnetic moment vector determined by using the right hand rule points in the +/- *y* direction. The torque on the magnetic moment is calculated as a cross-product

with the main magnetic field direction (i.e. along z), the torque must be parallel to the x-axis. For every set of loops on the normally-operating Gy coil that represent a magnetic moment in the positive-y direction, there will be a set representing a moment in the negative-y direction. This results in a net zero torque under normal operation. When the Gy coil is translated, the magnitude of the torques will generally change as one end of the coil begins to enter a region of reduced magnetic field strength. This will result in a net torque on the coil as it nears the extremes of the magnet bore. For a coil with a quadrant short, one of the magnetic moments clearly becomes zero and the coil will experience a non-zero net torque even while located at the center of the magnet. Regardless of these scenarios, the direction of torque for the Gy coil (with no rotation) will always be along the x direction.

From figure 3.12b the peak torque occurs when the coil centre was located at (0 m, 0 m, 0.91 m). This locates the outermost windings at 0.81 m along the z-axis, or 30 cm from the cold bore limits. Ideally the largest torque would occur when the forces on the coil are at their most unbalanced, yet still large. When the coil is located closer to the bore of the magnet, the forces that cause the torque are the most unbalanced, but they are also smaller than the internal forces exerted with the coil is located closer to the center of the magnet. It makes sense that there is a trade-off between these two effects which results in the position of peak torque being observed somewhere in between these two extremes.

In this study, the transverse coils were always modeled as Gy axes. A Gx gradient axis simply represents a 90-degree azimuthal rotation of a Gy axis. As a result, all of the previous discussion for the Gy coils applies equally well to the Gx axis, with the difference being that Gx coils can only experience net torque along the y-direction.

A Gz coil is a collection of current carrying loops aligned in the xy-plane. With the magnetic moment for a circular loop in the xy plane being parallel with the main field, the cross product $\underline{\mu} \times \underline{B}$ will be zero resulting in no net torque on a Gz insert coil aligned with the main field, regardless of position and regardless of failure

mode. Only when the Gz coil is positioned at an angle with respect to the main magnetic field will a net torque result.

For a single loop of wire within a completely uniform magnetic field, there is no net translational force on the loop. The loop winding actually feels only a force directed radially outwards, tending to force the loop to expand. This is termed "hoop stress". A loop only feels a net translational force when placed within a non-zero magnetic field with a non-zero field gradient. This is obviously the case closer to the ends of the magnet. In these cases, the loop will experience a non-zero force that is either along the field gradient or opposed to it, depending on the relative current direction through the loop. As the Gz coil is essentially just a sum of many individual circular loops arranged longitudinally along the coil, it is clear that net forces are to be expected on the structure as it is positioned in the vicinity of the opening to the main magnet.

4.6 Safe Regions:

With so much data produced for force and torque under various failure modes and various positioning errors, we implemented a "Safe Region" summary plot. The idea was to plot a volume or set of volumes that can be considered safe for every operation mode and insert coil position investigated. This allowed the meaningful data from every coil operation mode and rotation to be displayed on a single plot.

4.6.1 Safe Region Thresholds:

In order to determine the extent of a Safe Region for a given coil, a maximum allowable force and torque had to be determined. A key variable in this evaluation is the mass of a coil. The assumption was made that for structural reasons all insert

coils would be potted in an epoxy compound. For this study it was assumed that the majority of the mass of an insert coil came from this epoxy material. It was also assumed that potting a coil increased the outer radius of that coil by 10 cm. Assuming a typical density of 2 g/cm^3 for thermally conductive epoxy [5], the mass of each coil could be estimated.

The maximum allowable safe force was chosen to be 10 % the force of gravity on the coil, using the mass of the coil as determined above. It was desired that the threshold would be some fraction of the force of gravity on the insert coil, because with a threshold set to less than the force of gravity, an insert coil in the Safe Region will not be at risk to lift due to the Lorentz force. The choice of 10% gravity is somewhat arbitrary. If the force threshold was increased, the size of the Safe Regions would become larger.

The maximum allowable torque was chosen to be 10 % the force of gravity applied at a distance of 1 m from the centre of mass of coil. All of the torque calculations were evaluated about the centre of mass of the insert coil, and when determining the threshold it was assumed that this torque was applied about a pivot a distance of 1 m from the centre of mass of the coil. This estimation could be improved by choosing a pivot point for the insert coil as the location that the coil would have to rotate around when acted upon by an external force. The most likely place would be at the physical edge of the insert, and so any coil rotation would simulate the insert lifting off the main magnet. The effects of having the torque effectively applied at a distance of 1 m is more conservative than if the pivot point was chosen as an edge of the insert coil.

4.6.2 Safe Regions:

In this section the Safe Regions for Force and Torque, as well as the global Safe Region results for each coil type will be discussed. The global Safe Region represents the locations of centre of mass where both the Lorentz force, and the

torque due to the Lorentz force are small enough to cause neither motion nor rotation respectively.

For all of the coil types and radii considered, the Safe Region - Force enclosed the isocentre of the main magnet. Except for the 20 cm radius Gy coil each Safe Region - Force had the two secondary safe regions beyond the ends of the magnet bore. This means that if the insert coil centre of mass was located near the magnet isocentre, then for any failure mode or orientation investigated the Lorentz force on the insert coil was small enough that coil operation can be considered safe. On the other hand, the locations that are most dangerous are when the coil was just outside of the entrance to the magnet bore. It is therefore critical to avoid any possibility of energizing insert gradient coils when they are being installed or removed from the scanner.

For every coil radii and type investigated, the Safe Region – Torque also enclosed the region in the vicinity of the centre of the main magnet, and extended to, or very close to, the limits of the bore.

When the centre of mass locations were allowed to vary from -5 m to 5 m, from figure 3.26, it can be seen that the Safe Regions extend to include the regions further from the main magnet. This is of course obvious, in that a gradient coil's operation must be safe when taken sufficiently far from the main magnet. The important observation is that, across all coil designs, once an insert coil is positioned with its center of mass within approximately 1.6m of the center of the magnet, the forces and torques could become significant. Beyond that distance, there is essentially little concern.

4.6.3 Further Discussion:

The maximum allowable force on an insert coil was chosen to be 10 % the force of gravity on the coil. When deciding if this is reasonable, the direction that the

Lorentz force was applied should be considered. If the Lorentz force is in the vertical direction, than a 10 % threshold would be quite conservative. If the resultant force was in the z-direction and therefore tended to cause the coil to move out of or into the magnet, this threshold might not be sufficient. In order for the coil to move then the Lorentz force applied would have to be greater than the friction (assuming that no other fixation is being used to keep the coil within the magnet). If the insert was to remain stationary then $F_L < \mu_s N$, where F_L was the Lorentz force and N was the normal force. With a 10 % force of gravity threshold on the insert coil, than $F_L = 0.10*m*g$. In the cases were this statement does not hold, then motion of the coil may occur if $\mu_s < 0.10$. Using a table of common values [4], the static coefficient of friction for Teflon on Teflon and Teflon on steel was 0.04. If these materials are used to move the coil into position, then it would be suggested that some other material, such as a rubber mat, be placed underneath the insert coil as a stopping mechanism.

When trying to determine the Lorentz force on the insert coils due to the main magnet, the magnetic field profile produced was the dominating source of error. While the main magnet presented did display high field uniformity over the region of interest, it was still a theoretical design. In an effort to improve this, the field could be measured in a desired system over a spatial region, and then these values could be used for any force and torque calculations in the future. Interpolation methods can be used to find the field at locations that were not measured experimentally.

4.7 Conclusion:

In summary, every insert coil investigated was shown to have safe operation when the insert coils centre of mass was near the isocentre of the main magnet. This was even for catastrophic failure modes and very large mis-positions and alignments. It was also found that for coil locations further than approximately

1.6 m from the center of the magnet, no dangerous forces or torques were expected. This clearly identifies a "region of concern" when it comes to the operation of insert gradient coils: coils positioned in the vicinity of the entrance to the magnet bore are by far the most dangerous. In future gradient insert work, precautions should be focused to prevent coil operation while located in this region.

References:

[1]:Cheng, Yu-Chun N. et al (2004). A Comparison of Two Design Methods for MRI Magnets. *IEEE Transactions on Applied Superconductivity, 14*(3), 2008-2014

[2]: De Bever, Joshua T. (2007). *Multiple-Imaging-Region Gradient Coil Insert for Parallel Imaging of Mice in MRI.* Unpublished masters dissertation, University of Western Ontario, Canada.

[3]: Chronik, Blaine A. et al (1998). Constrained Length Minimum Inductance Gradient Coil Design. *Magnetic Resonance in Medicine, 39*, 270-278.

[4]: Chronik, Blaine A., Alejski, Andrew, Rutt, Brian K. (2000). Design and Fabrication of a Three-Axis Edge ROU Head and Neck Gradient Coil. *Magnetic Resonance in Medicine, 44*, 955-963

[5]:"Epoxies.com". 50-3100 High Thermal K Heat Transfer Epoxy Resin. http://www.epoxies.com/therm.htm (Aug 13/09)

[6]: Young, Hugh D et al (2004). *University Physics 11th Edition.* Toronto: Pearson Addison Wesley